KEK-TH-1236
OCHA-PP-298

arXiv:1104.1769v2 [hep-ph] 24 Oct 2011

The MSSM confronts the precision electroweak data and the muon $g-2$

Gi-Chol Cho[a], **Kaoru Hagiwara**[b,c], **Yu Matsumoto**[a,b] and **Daisuke Nomura**[d]

[a] *Department of Physics, Ochanomizu University, Tokyo 112-8610, Japan*
[b] *KEK Theory Center, Tsukuba 305-0801, Japan*
[c] *Sokendai, Tsukuba 305-0801, Japan*
[d] *Department of Physics, Tohoku University, Sendai 980-8578, Japan*

Abstract

We update the electroweak study of the predictions of the Minimal Supersymmetric Standard Model (MSSM) including the recent results on the muon anomalous magnetic moment, the weak boson masses, and the final precision data on the Z boson parameters from LEP and SLC. We find that the region of the parameter space where the slepton masses are a few hundred GeV is favored from the muon $g-2$ for $\tan\beta \lesssim 10$, whereas for $\tan\beta \simeq 50$ heavier slepton mass up to ~ 1000 GeV can account for the reported $3.2\,\sigma$ difference between its experimental value and the Standard Model (SM) prediction. As for the electroweak measurements, the SM gives a good description, and the sfermions lighter than 200 GeV tend to make the fit worse. We find, however, that sleptons as light as 100 to 200 GeV are favored also from the electroweak data, if we leave out the jet asymmetry data that do not agree with the leptonic asymmetry data. We extend the survey of the preferred MSSM parameters by including the constraints from the $b \to s\gamma$ transition, and find favorable scenarios in the minimal supergravity, gauge-, and mirage-mediation models of supersymmetry breaking.

1 Introduction

Despite anticipation that physics beyond the Standard Model (SM) should show up at energies just above the reach of the present collider experiments, we have so far been unsuccessful in identifying the nature of new physics. Supersymmetric (SUSY) extensions of the SM, in particular, the minimal supersymmetric standard model (MSSM) has several attractive features, such as the unification of the three gauge couplings. In Ref. [1], two of us performed a comprehensive study of constraints on the MSSM parameters from precision electroweak (EW) experiments by using the data published in 1999 [2]. It was found that almost all SUSY particle masses are constrained to be larger than a few 100 GeV, except for the light wino-like chargino whose contribution improved the SM fit slightly.

Since then, there have been several improvements in the EW measurements and theoretical analyses. Most notably, the LEP results have been finalized [3, 4] and the estimate of the running QED coupling constant at the Z boson mass scale has been improved by the contribution from the BES experiment [5, 6]. Also, the measurements of the muon anomalous magnetic moment at BNL have been finalized [7], and a 3.2 σ discrepancy from the SM prediction has been reported [8] (see Refs. [9–11] for the determination of the hadronic contribution to the muon $g-2$ from other groups). Those changes in the EW data, the W boson mass data [12, 13] and the top-quark mass data [13, 14] lead to new constraints on the MSSM parameters. On theory side, a number of groups have studied the EW fits in the SM and in the MSSM: for reviews, see e. g. Ref. [15]. Refs. [16–18] update the constraints on the Higgs boson mass in the SM using the EW data as well as the LEP and the Tevatron data for direct searches for the SM Higgs boson. Ref. [19] provides a comprehensive analysis of the MSSM EW precision fits using the state-of-the-art multi-loop calculations of the EW precision observables [20]. The EW precision fits in the minimal supergravity mediated SUSY breaking (mSUGRA) scenarios have been studied in many papers [21–47]. They are also studied in the split SUSY model [42, 48], in the gauge- [27, 28, 33, 42, 47, 49], anomaly- [28, 33, 42], moduli- [28, 50], and radion mediations [42], in the supergravity models with non-universal gaugino masses [51] and with non-universal Higgs masses [26, 52] and in the 25-parameter "phenomenological MSSM" model [53]. The EW observables in the MSSM are also studied in attempts to accommodate the NuTeV anomaly [54, 55] and the discrepancy between the effective Weinberg angles extracted from the leptonic and hadronic asymmetries [56].

Another advance on the theory side is a deeper understanding of the jet asymmetries measured at the LEP experiments. In Ref. [57], QCD radiative corrections to the jet asymmetries are studied, and it is argued that in the final report of the LEP experiments [3] the systematic errors of the jet asymmetries might have been underestimated. This is also a part of the motivation to revisit the EW fits in this paper.

In this paper, we present quantitative results based on the muon $g-2$ and the final EW data from LEP and SLC [3, 4]. In section 2, we discuss the MSSM contribution to the muon $g-2$, and identify its preferred parameter region. In section 3, we give our parametrization of the EW observables at the Z-pole and the mass and the width of the W boson in the SM. In section 4, we briefly review the MSSM contributions to the EW precision observables. In section 5, we explore a few SUSY breaking models and identify several preferred scenarios that can accommodate also the $b \to s\gamma$ rate. Section 6 gives summary and discussions.

2 The muon $g-2$ vs MSSM

2.1 The muon $g-2$ in the MSSM

The muon $g-2$ is a precisely measured quantity, and hence it is an excellent probe of new physics at the TeV scale. The measurement at BNL was finalized in 2006 [7]. After including a small shift in the value of the proton-to-muon magnetic ratio reported since then [58], the experimental value is [13]:

$$a_\mu^{\rm exp} = 11659208.9(6.3) \times 10^{-10}. \tag{1}$$

As for the SM prediction, the recent improvement in the low-energy $e^+e^- \to$ hadrons data from BaBar [59], BES [6], CMD-2 [60], KLOE [61, 62] and SND [63] allows us to reduce the uncertainty. In Ref. [8], the SM prediction has been evaluated as (after correcting a typo in Ref. [8]),

$$a_\mu^{\rm SM} = 11659183.0(5.1) \times 10^{-10}, \tag{2}$$

which includes all the major updates on the $e^+e^- \to$ hadrons data, and adopts the estimate [64], $a_\mu^{\rm l\text{-}by\text{-}l} = 10.5(2.6) \times 10^{-10}$, for the light-by-light contribution. Other independent analyses [9, 10, 11] based on the e^+e^- data give similar estimates. Hence, the observed value of the muon $g-2$ is larger than the SM prediction by

$$\delta a_\mu \equiv a_\mu^{\rm exp} - a_\mu^{\rm SM} = (25.9 \pm 8.1) \times 10^{-10}, \tag{3}$$

which differs from zero by 3.2 σ. It is tempting to interpret the difference as a contribution of new particles with the muon quantum number, such as smuons in the SUSY SM. Throughout this article we assume that the MSSM contribution accounts for this discrepancy.

In the MSSM, the contribution to the muon $g-2$ has been calculated up to and including the two-loop level [65]. In view of the smallness of the two-loop contribution, in this paper we restrict our analyses in the one-loop approximation[1].

At one-loop, the MSSM contribution comes from the chargino contribution $a_\mu(\widetilde{\chi}^-)$ and the neutralino contribution $a_\mu(\widetilde{\chi}^0)$. The relevant one-loop expressions in the notation of Ref. [1] are found e.g. in Refs. [67, 68], as:

$$\begin{aligned} a_\mu(\widetilde{\chi}^-) = \frac{1}{8\pi^2}\frac{m_\mu}{m_{\widetilde{\nu}_\mu}}\sum_{j=1}^{2}\Bigg\{&\left(\left|g_L^{\widetilde{\chi}_j^-\mu\widetilde{\nu}_\mu}\right|^2 + \left|g_R^{\widetilde{\chi}_j^-\mu\widetilde{\nu}_\mu}\right|^2\right)\frac{m_\mu}{m_{\widetilde{\nu}_\mu}} G_1\left(\frac{m^2_{\widetilde{\chi}_j^-}}{m^2_{\widetilde{\nu}_\mu}}\right) \\ &+ {\rm Re}\left[\left(g_R^{\widetilde{\chi}_j^-\mu\widetilde{\nu}_\mu}\right)^* g_L^{\widetilde{\chi}_j^-\mu\widetilde{\nu}_\mu}\right]\frac{m_{\widetilde{\chi}_j^-}}{m_{\widetilde{\nu}_\mu}} G_3\left(\frac{m^2_{\widetilde{\chi}_j^-}}{m^2_{\widetilde{\nu}_\mu}}\right)\Bigg\}, \end{aligned} \tag{4a}$$

$$\begin{aligned} a_\mu(\widetilde{\chi}^0) = -\frac{1}{8\pi^2}\sum_{i=1}^{2}\frac{m_\mu}{m_{\widetilde{\mu}_i}}\sum_{j=1}^{4}\Bigg\{&\left(\left|g_L^{\widetilde{\chi}_j^0\mu\widetilde{\mu}_i}\right|^2 + \left|g_R^{\widetilde{\chi}_j^0\mu\widetilde{\mu}_i}\right|^2\right)\frac{m_\mu}{m_{\widetilde{\mu}_i}} G_2\left(\frac{m^2_{\widetilde{\chi}_j^0}}{m^2_{\widetilde{\mu}_i}}\right) \\ &+ {\rm Re}\left[\left(g_R^{\widetilde{\chi}_j^0\mu\widetilde{\mu}_i}\right)^* g_L^{\widetilde{\chi}_j^0\mu\widetilde{\mu}_i}\right]\frac{m_{\widetilde{\chi}_j^0}}{m_{\widetilde{\mu}_i}} G_4\left(\frac{m^2_{\widetilde{\chi}_j^0}}{m^2_{\widetilde{\mu}_i}}\right)\Bigg\}, \end{aligned} \tag{4b}$$

[1] The effect from the $\tan\beta$-enhanced resummation in the muon-muon-Higgs vertex can change the MSSM contribution by about 10% [66], which does not affect the conclusions in the present paper significantly.

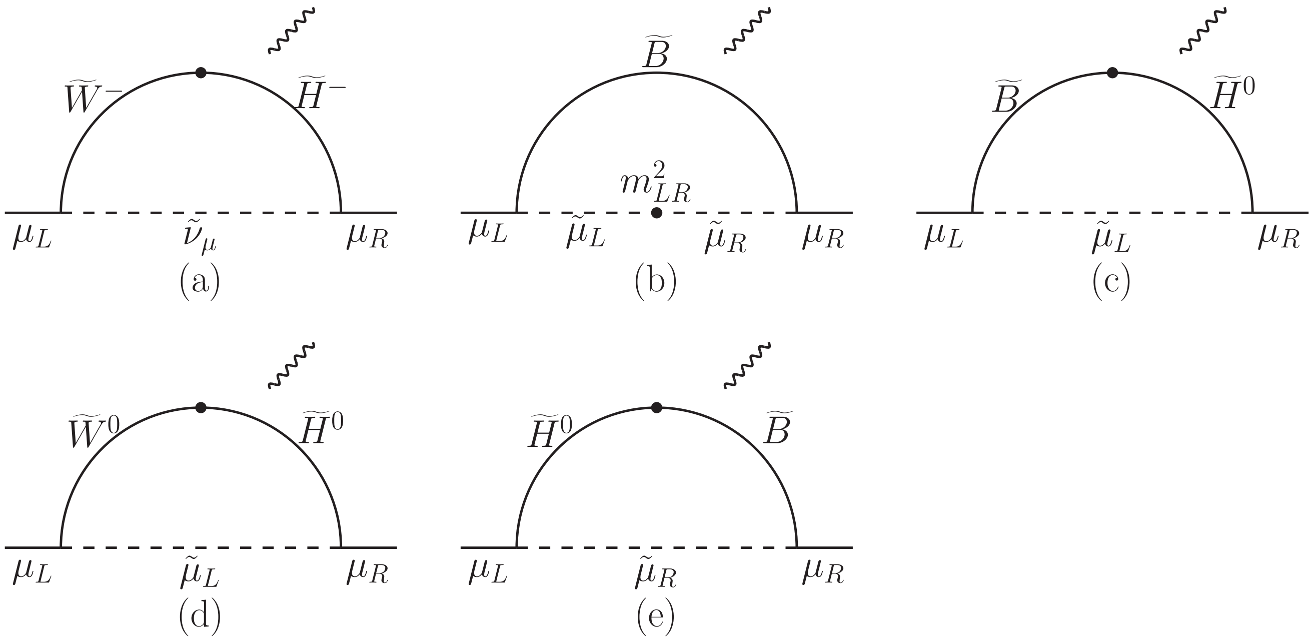

Figure 1: The SUSY contributions to the muon $g-2$ which give the leading terms of the expansion in $m_Z/m_{\rm SUSY}$. The photon (wavy line) is attached to all the charged particles.

where

$$G_1(x) = \frac{1}{12(x-1)^4}\left[(x-1)(x^2-5x-2)+6x\ln x\right] , \tag{5a}$$

$$G_2(x) = \frac{1}{12(x-1)^4}\left[(x-1)(2x^2+5x-1)-6x^2\ln x\right] , \tag{5b}$$

$$G_3(x) = \frac{1}{2(x-1)^3}\left[(x-1)(x-3)+2\ln x\right] , \tag{5c}$$

$$G_4(x) = \frac{1}{2(x-1)^3}\left[(x-1)(x+1)-2x\ln x\right] . \tag{5d}$$

Even though these expressions are useful for numerical calculations, they are not particularly illuminating for the purpose of understanding their dependences on the SUSY parameters. The main disadvantage of the above expressions is that they are written in terms of the mass eigenstates, in terms of which the dependences on the SUSY breaking parameters are hidden by the electroweak symmetry breaking that causes complex mixings.

In the weak eigenstates, the structure of the one-loop contributions becomes much more transparent. This simplification occurs since the expressions in the weak eigenstates are equivalent to the $m_Z/m_{\rm SUSY}$ expansion, where $m_{\rm SUSY}$ is the typical SUSY breaking mass scale. The price we have to pay is that the leading terms in the expansion are not useful when $m_{\rm SUSY} \sim m_Z$. However, we will find below that this expansion is very useful when analyzing the SUSY parameter dependence.

The leading terms in the $m_Z/m_{\rm SUSY}$ expansion are given by the five diagrams (a) to (e)

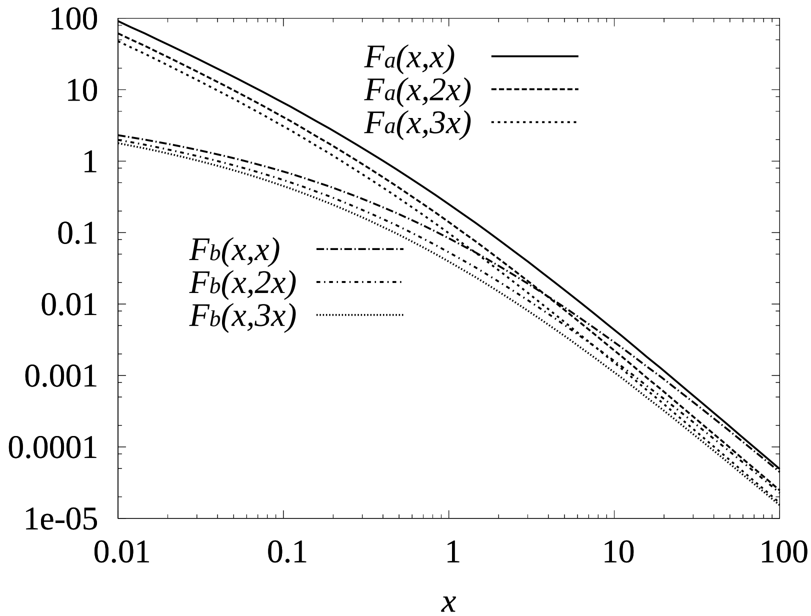

Figure 2: The behaviors of the functions $F_a(x,y)$ and $F_b(x,y)$, which appear in SUSY contributions to the muon $g-2$, for $y = x, 2x, 3x$.

in Fig. 1, whose contributions can be expressed compactly as

$$a_\mu(\tilde{W}\text{-}\tilde{H}, \tilde{\nu}_\mu) = \frac{g^2}{8\pi^2}\frac{m_\mu^2 M_2 \mu \tan\beta}{m_{\tilde{\nu}}^4}\, F_a\left(\frac{M_2^2}{m_{\tilde{\nu}}^2}, \frac{\mu^2}{m_{\tilde{\nu}}^2}\right), \tag{6a}$$

$$a_\mu(\tilde{B}, \tilde{\mu}_L\text{-}\tilde{\mu}_R) = \frac{g_Y^2}{8\pi^2}\frac{m_\mu^2 \mu \tan\beta}{M_1^3}\, F_b\left(\frac{m_{\tilde{\mu}_L}^2}{M_1^2}, \frac{m_{\tilde{\mu}_R}^2}{M_1^2}\right), \tag{6b}$$

$$a_\mu(\tilde{B}\text{-}\tilde{H}, \tilde{\mu}_L) = \frac{g_Y^2}{16\pi^2}\frac{m_\mu^2 M_1 \mu \tan\beta}{m_{\tilde{\mu}_L}^4}\, F_b\left(\frac{M_1^2}{m_{\tilde{\mu}_L}^2}, \frac{\mu^2}{m_{\tilde{\mu}_L}^2}\right), \tag{6c}$$

$$a_\mu(\tilde{W}\text{-}\tilde{H}, \tilde{\mu}_L) = -\frac{g^2}{16\pi^2}\frac{m_\mu^2 M_2 \mu \tan\beta}{m_{\tilde{\mu}_L}^4}\, F_b\left(\frac{M_2^2}{m_{\tilde{\mu}_L}^2}, \frac{\mu^2}{m_{\tilde{\mu}_L}^2}\right), \tag{6d}$$

$$a_\mu(\tilde{B}\text{-}\tilde{H}, \tilde{\mu}_R) = -\frac{g_Y^2}{8\pi^2}\frac{m_\mu^2 M_1 \mu \tan\beta}{m_{\tilde{\mu}_R}^4}\, F_b\left(\frac{M_1^2}{m_{\tilde{\mu}_R}^2}, \frac{\mu^2}{m_{\tilde{\mu}_R}^2}\right), \tag{6e}$$

respectively. The functions $F_a(x,y)$ and $F_b(x,y)$ are defined as:

$$F_a(x,y) \equiv -\frac{G_3(x) - G_3(y)}{x-y}, \qquad F_b(x,y) \equiv -\frac{G_4(x) - G_4(y)}{x-y}, \tag{7}$$

which are symmetric under exchange of the two arguments. The functions $G_3(x)$ and $G_4(x)$ are monotonically decreasing for $0 < x < \infty$, and hence the functions $F_a(x,y)$ and $F_b(x,y)$ are positive for all positive x and y. In Fig. 2, we show the behaviors of $F_{a,b}(x,nx) = F_{a,b}(nx,x)$ for $n = 1,\ldots,3$.

The expressions (6a)-(6e) allow us to make a few general observations on the SUSY parameter dependences. The first one is that the contributions from the diagrams (a)-(c)

in Fig. 1 are positive, while those from the diagrams (d) and (e) are negative for $M_2\mu$ and $M_1\mu > 0$. In addition, if the mass-splitting in the $(\tilde{\nu}_\mu, \tilde{\mu}_L)$ doublet is small we can conclude that the sum of the diagrams (a) and (d), or that of Eqs. (6a) and (6d) is always positive, because $F_a(x, y)$ is always larger than $F_b(x, y)$ for the same arguments as shown in Fig. 2. If the contributions from the diagrams (b), (c), and (e) are suppressed, being proportional to $g_Y^2 = g^2 \tan^2\theta_W$, we can conclude that $M_2\mu$ should be positive in order to explain the positive deviation of the muon $g-2$ from the SM prediction in Eq. (3).

In fact, the only way to obtain a positive MSSM contribution for $M_1\mu < 0$ and $M_2\mu < 0$ is to make the contribution from the diagram (e), Eq. (6e), dominates over the others, which requires $(M_2/m_{\tilde{L}}^4) F_a(M_2^2/m_{\tilde{L}}^2, \mu^2/m_{\tilde{L}}^2) \ll \tan^2\theta_W (M_1/m_{\tilde{E}}^4) F_b(M_1^2/m_{\tilde{E}}^2, \mu^2/m_{\tilde{E}}^2)$. This situation is realized for $|M_1|, m_{\tilde{E}} \ll |M_2|, m_{\tilde{L}}$: for instance, when $(\tan\beta, \mu, m_{\tilde{E}}, m_{\tilde{L}}, M_2, M_1) = (50, -300, 120, 1200, 1000, 100)$, where the mass dimension is counted in units of GeV, the diagram (e) dominates over the others, and the predicted value of a_μ is within the 1-σ favored region. In this example, an $M_1\mu < 0$ solution is realized by setting $M_2/M_1 = m_{\tilde{L}}/m_{\tilde{E}} = 10$. We find that all the solutions with $M_1\mu < 0$ require both $|M_2/M_1| \gg 1$ and $m_{\tilde{L}}/m_{\tilde{E}} \gg 1$. However, as discussed later, scenarios with heavy left-handed sleptons do not lead to a significant signal in the electroweak precision measurements, and we do not consider such scenarios hereafter.

Another interesting observation is that in the case where μ is large as compared to the SUSY breaking soft mass parameters, the contributions from the diagrams (a) and (c)-(e) are suppressed by $1/\mu$, as manifestly shown by the Higgsino propagator in the diagrams Figs. 1 (a) and (c)-(e). On the other hand, the diagram (b) is proportional to μ, which makes this contribution important.

The above observations can be made explicit by neglecting the D-term and the F-term contributions to the slepton mass matrices, which makes $m_{\tilde{\mu}_L} = m_{\tilde{\nu}} = m_{\tilde{L}}$ and $m_{\tilde{\mu}_R} = m_{\tilde{E}}$, where $m_{\tilde{L}}$ and $m_{\tilde{E}}$ are the left-handed and the right-handed slepton soft SUSY breaking masses, respectively. Then, Eqs. (6a)-(6e) simplify as

$$a_\mu(\tilde{W}\text{-}\tilde{H}, \tilde{\nu}_\mu) = a_\mu^{\text{ref}} \cdot F_a\left(\frac{M_2^2}{m_{\tilde{L}}^2}, \frac{\mu^2}{m_{\tilde{L}}^2}\right), \tag{8a}$$

$$a_\mu(\tilde{B}, \tilde{\mu}_L\text{-}\tilde{\mu}_R) = a_\mu^{\text{ref}} \cdot \tan^2\theta_W \frac{m_{\tilde{L}}^4}{M_1^3 M_2} F_b\left(\frac{m_{\tilde{L}}^2}{M_1^2}, \frac{m_{\tilde{E}}^2}{M_1^2}\right), \tag{8b}$$

$$a_\mu(\tilde{B}\text{-}\tilde{H}, \tilde{\mu}_L) = a_\mu^{\text{ref}} \cdot \frac{1}{2} \tan^2\theta_W \frac{M_1}{M_2} F_b\left(\frac{M_1^2}{m_{\tilde{L}}^2}, \frac{\mu^2}{m_{\tilde{L}}^2}\right), \tag{8c}$$

$$a_\mu(\tilde{W}\text{-}\tilde{H}, \tilde{\mu}_L) = -a_\mu^{\text{ref}} \cdot \frac{1}{2} F_b\left(\frac{M_2^2}{m_{\tilde{L}}^2}, \frac{\mu^2}{m_{\tilde{L}}^2}\right), \tag{8d}$$

$$a_\mu(\tilde{B}\text{-}\tilde{H}, \tilde{\mu}_R) = -a_\mu^{\text{ref}} \cdot \tan^2\theta_W \frac{M_1 m_{\tilde{L}}^4}{M_2 m_{\tilde{E}}^4} F_b\left(\frac{M_1^2}{m_{\tilde{E}}^2}, \frac{\mu^2}{m_{\tilde{E}}^2}\right), \tag{8e}$$

where

$$a_\mu^{\text{ref}} \equiv \frac{g^2}{8\pi^2} \frac{m_\mu^2 M_2 \mu \tan\beta}{m_{\tilde{L}}^4}. \tag{9}$$

Only for the above specific scenario with $m_{\tilde{L}}/m_{\tilde{E}} \gg 1$ and $|M_2/M_1| \gg 1$, Eq. (8e) dominates over the others and $M_1\mu < 0$ is required to account for the positive shift, Eq. (3). In the very heavy Higgsino case with $|\mu/M_1|, |\mu/M_2| \gg 1$, Eq. (8b) dominates, and $M_1\mu > 0$ is necessary to account for the positive shift. Except for the above two cases, Eq. (8a) dominates, and $M_2\mu > 0$ follows.

We note that the above discussion on the favored signs of $M_1\mu$ and $M_2\mu$ are valid equally for both positive and negative M_1 and M_2 since the signs of M_1 and M_2 enter only through the combinations $M_1\mu$ and $M_2\mu$. In particular, we can use the same argument to identify the favored signs of $M_1\mu$ and $M_2\mu$ also for a model with $\mathrm{sgn}(M_1) = -\mathrm{sgn}(M_2)$, which is realized in some parameter regions of the mixed moduli and anomaly mediation model [69].

A comment on the SUSY breaking tri-linear coupling A_μ is in order here. In the one-loop order, the parameter A_μ enters only through the $\tilde{\mu}_L$-$\tilde{\mu}_R$ mixing in the combination $(A_\mu^* - \mu \tan\beta)$ in the diagram Fig. 1 (b). In order for A_μ to affect the muon $g-2$ significantly, Fig. 1 (b) should dominate over the others, but it implies large $|\mu|$ according to the above discussions. Since there is no attractive SUSY breaking scenarios that lead to a huge magnitude of $|A_\mu| \sim |\mu| \tan\beta$, and since moderate values of $|A_\mu| \lesssim |\mu|$ do not affect the qualitative behavior, we set $A_\mu = 0$ in the following, unless otherwise stated[2].

In Fig. 3 we show contour plots of the SUSY contribution to the muon $g-2$ as a function of the right-handed slepton mass $m_{\tilde{E}}$ and the $SU(2)_L$ gaugino mass M_2. In the figures, we examine the four combinations of $\tan\beta$ and μ; $\tan\beta = 10$ or 50 and $\mu = 200$ or 800 GeV. As for the other relevant SUSY parameters, we assume the gaugino mass unification condition, $M_1/M_2 = (5/3)\tan^2\theta_W$, and the left-handed slepton mass is taken to be equal to the right-handed slepton mass, for simplicity. Under these assumptions, we plot, from the lower left corner, the $+3\sigma$, $+2\sigma$, $+1\sigma$, -1σ and -2σ contours. (We do not plot -3σ curves since those lie outside of the panel for Fig. 3(a), (b), (c) and (d)). The area surrounded by the $\pm 1\sigma$ contours is shaded. The vertical dotted lines give the lower bound on M_2 beyond which the lightest chargino mass becomes less than the experimental limit, 103.5 GeV [71]. Also shown by the horizontal dotted lines are the stau mass limit, 81.9 GeV [13]. We also show the contour of a constant "electroweak χ^2 factor", defined as the squared sum of the SUSY contributions to the electroweak S_Z- and T_Z-parameters [1] and to m_W;

$$\Delta\chi^2_{\mathrm{EW}} = \left(\frac{(\Delta S_Z)_{\mathrm{SUSY}}}{0.04}\right)^2 + \left(\frac{(\Delta T_Z)_{\mathrm{SUSY}}}{0.04}\right)^2 + \left(\frac{(\Delta m_W)_{\mathrm{SUSY}}}{30\mathrm{MeV}}\right)^2 . \tag{10}$$

The parameter regions in the left-bottom side of the dash-dotted curves give $\Delta\chi^2_{\mathrm{EW}} > 0.5$, and there can be a hint of SUSY contributions to the electroweak observables in the near future[3]. See discussions in Section 4 for details.

In the figures, the sample points MSSM1–MSSM6 denoted by the cross symbols ($\times$), are chosen in the 1-σ allowed region of the muon $g-2$ where $\Delta\chi^2_{\mathrm{EW}} > 0.5$. They represent the two extreme cases where either a slepton (2,4,6) or an ino (1,3,5) is light. Our choices of μ and M_2 allow us to cover the cases where the lighter chargino is wino-like (3,4,5), Higgsino-like

[2] For the possibility of explaining the muon $g-2$ anomaly using a large A term, see e.g. Ref. [70].

[3] The "dips" in Figs. 3 (a) and (c) at $M_2 \simeq 120$GeV and 350 GeV $\lesssim m_{\tilde{E}} \lesssim 400$ GeV happen since around this region there is a destructive interference between the combination "$\Delta T - \Delta\overline{\delta}_G/\alpha$" and the ΔR_Z term in ΔT_Z (see eq. (16b)), which makes the contribution from ΔT_Z to $\Delta\chi^2_{\mathrm{EW}}$ small.

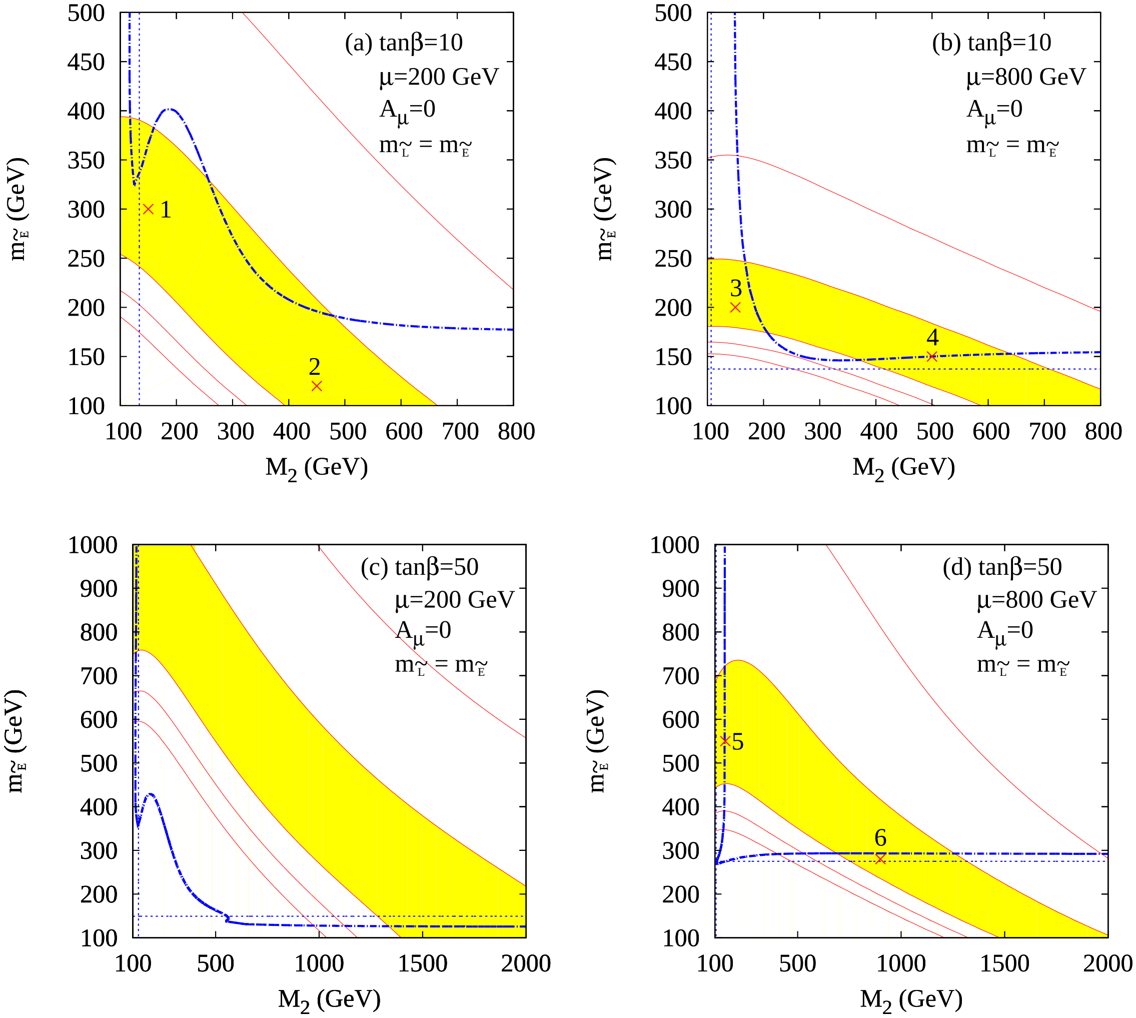

Figure 3: The muon $g-2$, plotted against M_2 (the $SU(2)_L$ gaugino mass) and $m_{\tilde{E}}$ (the right-handed smuon soft SUSY breaking mass) for $\tan\beta = 10$ (top two panels) and $\tan\beta = 50$ (bottom two panels), and for $\mu = 200$ GeV (left two panels) and $\mu = 800$ GeV (right two panels). The curves are, from the lower left corner, $+3\sigma$, $+2\sigma$, $+1\sigma$, -1σ and -2σ contour for the difference δa_μ between the data and the SM prediction. The region on the left-hand side of the vertical dotted line is excluded by the chargino mass limit $m_{\tilde{\chi}_1^-} > 103.5$ GeV [71], and the region below the horizontal dotted line is ruled out by the stau mass limit $m_{\tilde{\tau}_1} > 81.9$ GeV [13]. The region below or in the left-hand side of the dash-dotted curve gives $\Delta\chi^2_{\rm EW} > 0.5$ contribution to the electroweak observables, see Eq. (10). The sample points discussed in the main text are marked by the crosses ($\times$). In the figures, we assume $A_\mu = 0$, $m_{\tilde{L}} = m_{\tilde{E}}$ and $M_1/M_2 = (5/3)\tan^2\theta_W$.

(2), or mixed (1,6). We use these six MSSM sample points in the study of the electroweak observables in later sections. The choice that there is either a light ino or a light slepton is interesting in view of the electroweak study since if there is a light new particle with nonzero electroweak quantum numbers, the contribution to the S_Z- and T_Z-parameters [1] and to m_W can be significant.

For these sample points, we present separate contributions from individual diagrams and their sum in Table 1. In the table, we show the sum of the five terms in the column '(a)-(e)', and the total SUSY contribution obtained without using the $m_Z/m_{\rm SUSY}$ expansion in the column under 'total'. By comparing these two columns, we confirm for all the six cases that the leading terms in the $m_Z/m_{\rm SUSY}$ expansion give an excellent approximation. The last column shows the pull factor

$$\text{pull} = \frac{(\delta a_\mu)^{\rm SUSY} - \langle \delta a_\mu \rangle}{\Delta \delta a_\mu}, \tag{11}$$

where the mean $\langle \delta a_\mu \rangle$ and the error $\Delta \delta a_\mu$ are taken from Eq. (3).

For $\tan\beta = 10$ and $\mu = 200$ GeV shown in Fig. 3(a), the 1-σ allowed region is very roughly given by 550GeV$\lesssim 1.7 m_{\tilde{E}} + M_2 \lesssim$800 GeV. Here, the diagram (a) gives the dominant contribution, as can be read off from the rows 1 and 2 in Table 1, respectively, for the MSSM points 1 and 2.

For a larger μ like $\mu = 800$ GeV shown in Fig. 3(b), the allowed region becomes narrower, partly due to the heavier Higgsinos, and partly because of the constraint from the stau mass lower bound $m_{\tilde{\tau}} > 81.9$ GeV [13]. In the parameter region of Fig. 3(b), the diagram (b) becomes more important because all the other diagrams are suppressed by the heavy Higgsino mass, as discussed above. This can be explicitly verified from Table 1, in the rows 3 and 4. In the MSSM point 3, the suppression of the diagram (a) by $1/\mu$ is not strong enough and hence the diagram (a) is still as important as (b). In the MSSM point 4, the diagram (a) is less important since it is suppressed not only by $1/\mu$ but also by $1/M_2$.

In the $\tan\beta = 50$ case, the allowed parameter space becomes much wider as shown in Fig. 3(c) for $\mu = 200$ GeV and Fig. 3(d) for $\mu = 800$GeV. When $\mu \sim 200$ GeV, the favored SUSY masses are so large that there is no region which satisfies both the 1-σ favored range of the muon $g-2$ and $\Delta\chi^2_{\rm EW} > 0.5$. When $\mu \sim 800$ GeV, in Fig. 3(d), there appear two distinct regions of the parameters that satisfy both conditions. In the small M_2 region around the MSSM point 5, $M_2 \gtrsim 100$ GeV is allowed by the lighter chargino mass constraint, and $M_2 \lesssim$150 GeV gives $\Delta\chi^2_{\rm EW} > 0.5$. In the small $m_{\tilde{E}}$ region around the MSSM point 6, although $m_{\tilde{E}} \sim 300$ GeV, the lighter stau is as light as $\sim$100 GeV and it gives a sizable contribution to the ΔT-parameter, which makes $\Delta\chi^2_{\rm EW}$ non-negligible. As for the muon $g-2$, in the MSSM point 5, the large slepton mass suppresses the diagram (b) despite large μ, and the light wino makes the diagram (a) dominate over the other contributions. In the MSSM point 6, the large μ enhancement of the diagram (b) is more effective, while the diagram (a) is suppressed by the large wino mass M_2. As a result, the contributions from the diagrams (a) and (b) are comparable.

In summary, for the scenarios in which the SUSY contribution to the muon $g-2$ can be tested by the electroweak precision study, the diagrams (a) and/or (b) give dominant contribution to the muon $g-2$.

No.	$\tan\beta$	μ	M_2	$m_{\tilde{E}}$	(a)	(b)	(c)	(d)	(e)	(a)-(e)	total	pull
1	10	200	150	300	29.6	1.1	0.7	−2.9	−1.3	27.2	25.0	−0.1
2	10	200	450	120	27.5	8.8	3.3	−7.1	−6.7	25.9	25.9	0.0
3	10	800	150	200	14.3	16.2	0.6	−2.7	−1.3	27.1	27.1	0.1
4	10	800	500	150	6.9	21.3	1.0	−2.5	−2.1	24.7	24.3	−0.2
5	50	800	150	550	26.9	2.4	0.5	−2.6	−1.0	26.3	26.0	0.0
6	50	800	900	280	18.0	18.0	2.5	−5.9	−5.1	27.7	27.6	0.2

Table 1: The parameters for the MSSM sample points, MSSM1 to MSSM6 in Fig. 3, and the breakdown of their contributions to the muon $g-2$ in units of 10^{-10}. The parameters with the mass dimension are given in GeV units, and $A_\mu = 0$ is assumed for all the points. The numbers in the columns (a) to (e) are the contributions from the corresponding diagrams in Fig. 1, and the column '(a)-(e)' gives their sum. The numbers in the column 'total' are calculated without using the $m_Z/m_{\rm SUSY}$ expansion, which slightly differ from the sum of the five contributions. The last column gives the pull factor, Eq. (11).

2.2 The muon $g-2$ in selected SUSY breaking scenarios

In the previous subsection we have examined SUSY contributions to the muon $g-2$ without assuming specific SUSY breaking scenarios. In this subsection we examine several SUSY breaking scenarios that are consistent with the other constraints like the $b \to s\gamma$ decay rate, and discuss in detail their contributions to the muon $g-2$. We will later examine their predictions for the electroweak observables.

We take seven scenarios that predict the muon $g-2$ values within or very close to the 1-σ allowed region; a few sample points each from three SUSY breaking scenarios, namely, the minimal supergravity (SG) [73], the gauge mediation (GM) [74], and the mixed moduli-anomaly (MM) mediation [69, 75] models. We call those sample points SG1, SG2, GM1, GM2, MM1, MM2 and MM3, respectively.

The SG1 point is the mSUGRA sample point advocated as SPS1a$'$ in Ref. [76], whose main advantage is that it is compatible with all high-energy mass bounds and with the constraints from the muon $g-2$, $\mathrm{Br}(b \to s\gamma)$ and the dark matter relic density. The SG2 point is a modified version of the SPS4 point, which is a mSUGRA point with $\tan\beta = 50$ proposed in Ref. [77]. At SPS4 the unified gaugino mass $m_{1/2}$ is 300 GeV, while at SG2 we take $m_{1/2} = 650$ GeV so that it is closer to the region favored from the muon $g-2$ and $\mathrm{Br}(b \to s\gamma)$. By this change in $m_{1/2}$, the pull factors for the muon $g-2$ and $\mathrm{Br}(b \to s\gamma)$ are improved from 3.1 and −5.9 to −0.8 and −1.4, respectively.

As representatives of the gauge mediation, we take the GM1 and GM2 points: in GM1 $\tan\beta$ is large ($\tan\beta = 42$), while in GM2 it is moderate ($\tan\beta = 15$). At these points the lightest SUSY particle (LSP) is the gravitino, whose interactions are too weak to be relevant for the electroweak observables in the present paper. In the GM1 point, which is one of the points studied in Ref [78], the next-to-lightest SUSY particle (NLSP) is bino, while in GM2, which is suggested as SPS7 in Ref. [77], the NLSP is the stau. Both points fit well with the muon $g-2$ and $\mathrm{Br}(b \to s\gamma)$.

The MM1 and MM2 points are sample points from the mixed moduli-anomaly (MM)

	$\tan\beta$	μ	$m_{\tilde{\mu}_L}$	$m_{\tilde{\mu}_R}$	$(m^2_{\tilde{\tau}})_{\rm LR}$	A_μ	M_1	M_2	M_3	m_A
SG 1	10	396	181	116	$-(88)^2$	-445	103	193	572	425
SG 2	50	762	585	465	$-(261)^2$	-145	277	510	1424	566
GM 1	42	504	441	214	$-(194)^2$	25	181	339	900	513
GM 2	15	300	257	120	$-(90)^2$	-39	169	327	896	378
MM1	10	430	188	255	$-(92)^2$	-465	170	258	641	513
MM2	10	-572	253	108	$(103)^2$	245	-99	-248	-847	616
MM3	10	534	200	237	$-(102)^2$	509	224	173	877	631

	$m_{\tilde{u}_L}$	$m_{\tilde{u}_R}$	$m_{\tilde{d}_R}$	$m_{\tilde{t}_L}$	$m_{\tilde{t}_R}$	$(m^2_{\tilde{t}})_{\rm LR}$	$(m^2_{\tilde{b}})_{\rm LR}$
SG 1	526	507	505	471	388	$-(322)^2$	$-(153)^2$
SG 2	1345	1297	1292	1173	1062	$-(435)^2$	$-(435)^2$
GM 1	1329	1269	1263	1264	1165	$(215)^2$	$-(316)^2$
GM 2	861	831	829	836	780	$-(241)^2$	$-(153)^2$
MM1	610	589	546	556	465	$-(336)^2$	$-(159)^2$
MM2	785	796	823	689	585	$(397)^2$	$(184)^2$
MM3	758	731	807	705	616	$-(353)^2$	$-(183)^2$

Table 2: The values of the relevant SUSY parameters for the selected scenarios. The parameters with the mass dimension are given in GeV units. $(m^2_{\tilde{f}})_{\rm LR}$ ($\tilde{f} = \tilde{\tau}, \tilde{t}, \tilde{b}$) are the left-right mixing element in the mass-squared matrices of the sfermion $\tilde{f}$. As for the notation of the other SUSY parameters, we use that of Ref. [1].

	(a)	(b)	(c)	(d)	(e)	(a)-(e)	total	pull
SG 1	25.7	21.5	1.5	-5.2	-5.4	38.1	37.6	1.4
SG 2	20.0	4.8	1.0	-3.4	-2.8	19.5	19.4	-0.8
GM 1	34.6	11.7	1.4	-5.3	-9.2	33.2	33.0	0.9
GM 2	27.1	10.6	1.6	-5.0	-9.0	25.3	24.8	-0.1
MM1	19.4	7.2	1.4	-4.5	-1.9	21.7	21.7	-0.5
MM2	13.2	18.8	0.7	-2.7	-4.2	25.8	24.7	-0.1
MM3	19.6	7.9	1.1	-3.8	-1.8	23.0	23.1	-0.3

Table 3: SUSY contributions to the muon $g-2$ for our sample points in units of 10^{-10}. The numbers in the column 'total' are calculated without using the $m_Z/m_{\rm SUSY}$ expansion, which slightly differ from the sum of the numbers in the five columns (a) to (e). The last column gives the pull factor, Eq. (11).

mediated SUSY breaking scenario. In MM1, the parameter α, which parametrizes the ratio between the moduli and the anomaly mediations, is positive, while it is negative for MM2. In MM1 and MM2, the parameters (l_1, l_2, l_3), which parametrize the contributions from moduli to the gaugino masses, are taken to be $l_1 = l_2 = l_3 = 1$ so that it allows the "mirage unification" [69], namely the gaugino masses unify at a high scale which can be different from the GUT scale $\sim 10^{16}$ GeV. In the case of a positive (negative) α, the gaugino masses unify below (above) the GUT scale. We take another sample point, which we call MM3, from a variant of the MM scenario. At this point, we take $(l_1, l_2, l_3) = (1, 1/2, 1)$ so that wino is lighter than bino[4]. The wino LSP is an interesting possibility since the excess of the positron flux observed at PAMELA [82, 83] can be explained by the wino dark matter [84].

For the above seven scenarios we list in Table 2 the values of the relevant SUSY parameters. We only use the parameters in the slepton and ino sectors for the study of the muon $g-2$, but later we need the squark and the Higgs sectors for the studies of the EW precision observables and $\mathrm{Br}(b \to s\gamma)$.

The breakdown of the contributions to the muon $g-2$ at each point with respect to the diagrams is given in Table 3. The discussions in the previous section can be verified from the numbers in this table. For all our sample points, the diagram (a) gives an important contribution. For the points where smuons are relatively light compared to the gauginos or the Higgsinos, such as SG1 and MM2, the diagram (b) also gives a comparable or larger contribution than that of the diagram (a). For all the points, the diagrams (c)-(e) give only subdominant contributions.

The similarity of the SG1,...,MM3 points to MSSM1–6 can be discussed as follows. Since SG1 is similar to MSSM3 in the sense that it has a bit larger μ than the slepton and the ino masses, both diagrams (a) and (b) give important contributions. SG2 is similar to MSSM5 in μ and the slepton masses but with a heavier inos, and hence the overall size of the SUSY contribution is smaller. GM1 can be considered to be an interpolation of MSSM5 and 6, but with a smaller $\tan\beta$, and hence the diagram (a) is dominant with a slightly smaller contribution from (b). GM2 is a relative of MSSM2, and the breakdown is similar. GM1 and GM2 have a light right-handed slepton and a moderate-mass ($\sim$200 GeV) bino, which make the contribution from (e) more important than in other SUSY sample points. MM1, MM2 and MM3 are similar to MSSM3, even though they have smaller μ. At MM2, M_1 and $m_{\tilde{\mu}_R}$ are smaller than MM1 and MM3, which makes the diagram (b) more important than at these two points. At MM1 and MM3, μ is a bit smaller, and hence the diagram (b) becomes a bit less important than at MSSM3 and MM2.

In summary, similarly to the discussions in the previous subsection, the diagrams (a) and/or (b) give important SUSY contributions to the muon $g-2$ also in the selected SUSY breaking model points.

[4] In the original KKLT model [79], the allowed values of l_a $(a = 1, \ldots, 3)$ are 0 or 1. However, when there is a contribution from the dilaton to the gauge kinetic functions, it is possible to have different predictions for the gaugino masses from the $l_a = 0$ or $l_a = 1$ cases [80, 81]. Here we take into account such a possibility by allowing l_a to take a fractional value as an "effective value", instead of explicitly introducing the dilaton in the gauge kinetic functions.

3 The electroweak observables

In this section, we briefly review the electroweak observables in the framework of Refs. [1, 85], and update the parametrizations of the SM predictions.

The electroweak observables of the Z-pole experiments are expressed in terms of the effective Z boson couplings g_α^f [86] to f_α, where f denotes the quark/lepton species and α stands for their chirality. The summary of the observables in terms of the effective couplings g_α^f can be found, for example, in Refs. [1, 87]. A convenient parametrization of the effective couplings in generic $SU(2)_L \times U(1)_Y$ electroweak theories is given by [1]:

$$\begin{aligned}
g_L^\nu &= 0.50199 + 0.45250\Delta\bar{g}_Z^2 + 0.00469\Delta\bar{s}^2 + \Delta g_L^\nu, && (12a)\\
g_L^e &= -0.26920 - 0.24338\Delta\bar{g}_Z^2 + 1.00413\Delta\bar{s}^2 + \Delta g_L^e, && (12b)\\
g_R^e &= 0.23207 + 0.20912\Delta\bar{g}_Z^2 + 1.00784\Delta\bar{s}^2 + \Delta g_R^e, && (12c)\\
g_L^u &= 0.34675 + 0.31309\Delta\bar{g}_Z^2 - 0.66793\Delta\bar{s}^2 + \Delta g_L^u, && (12d)\\
g_R^u &= -0.15470 - 0.13942\Delta\bar{g}_Z^2 - 0.67184\Delta\bar{s}^2 + \Delta g_R^u, && (12e)\\
g_L^d &= -0.42434 - 0.38279\Delta\bar{g}_Z^2 + 0.33166\Delta\bar{s}^2 + \Delta g_L^d, && (12f)\\
g_R^d &= 0.07734 + 0.06971\Delta\bar{g}_Z^2 + 0.33590\Delta\bar{s}^2 + \Delta g_R^d, && (12g)\\
g_L^b &= -0.42116 - 0.38279\Delta\bar{g}_Z^2 + 0.33166\Delta\bar{s}^2 + \Delta g_L^b, && (12h)\\
g_R^b &= 0.07742 + 0.06971\Delta\bar{g}_Z^2 + 0.33590\Delta\bar{s}^2 + \Delta g_R^b, && (12i)
\end{aligned}$$

where the mean values denote the SM predictions for $m_t = 172$ GeV, $m_{H_{\rm SM}} = 100$ GeV, $\Delta\alpha_{\rm had}^{(5)}(m_Z^2) = 0.0277$ and $\hat{\alpha}_s(m_Z)_{5q} = 0.118$, and the coefficients of $\Delta\bar{g}_Z^2$ and $\Delta\bar{s}^2$ control the dependences on the oblique (gauge boson propagator) corrections. Here, $\Delta\bar{g}_Z^2$ and $\Delta\bar{s}^2$ are the universal gauge-boson-propagator corrections [87] to the effective Z-boson couplings and the Z-γ mixing at the m_Z scale, respectively, and Δg_α^f denote the shifts due to vertex corrections. In the SM, only $(\Delta g_L^b)_{\rm SM}$ and $(\Delta g_R^b)_{\rm SM}$ have non-trivial m_t and $m_{H_{\rm SM}}$ dependence, and the others do not receive m_t- or $m_{H_{\rm SM}}$-dependent one-loop contribution. On the other hand, all the Δg_α^f terms are non-vanishing at the one-loop level in the MSSM.

The universal part of the corrections, $\Delta\bar{g}_Z^2$ and $\Delta\bar{s}^2$, are defined as the shift in the effective couplings $\bar{g}_Z^2(m_Z^2)$ and $\bar{s}^2(m_Z^2)$ [87] from their SM reference values at $(m_t, m_{H_{\rm SM}}, \Delta\alpha_{\rm had}^{(5)}(m_Z^2))$ = (172 GeV, 100 GeV, 0.0277):

$$\begin{aligned}
\bar{g}_Z^2(m_Z^2) &= 0.55602 + \Delta\bar{g}_Z^2, && (13a)\\
\bar{s}^2(m_Z^2) &= 0.23048 + \Delta\bar{s}^2. && (13b)
\end{aligned}$$

The shifts in the two effective couplings can conveniently be expressed in terms of the parameters ΔS_Z, ΔT_Z and x_α,

$$\begin{aligned}
\Delta\bar{g}_Z^2 &= 0.00412\Delta T_Z, && (14a)\\
\Delta\bar{s}^2 &= 0.00360\Delta S_Z - 0.00241\Delta T_Z + 0.00011 x_\alpha. && (14b)
\end{aligned}$$

Here the parameter x_α,

$$x_\alpha \equiv \frac{\Delta\alpha_{\rm had}^{(5)}(m_Z^2) - 0.0277}{0.0003}, \tag{15}$$

measures the $\alpha(m_Z^2)$ dependence of the effective mixing parameter $\bar{s}^2(m_Z^2)$. The parameters ΔT_Z and ΔS_Z denote the shift of S_Z and T_Z from their values at the SM reference point, and are related to the S- and T-parameters as [88]:

$$\Delta S_Z = \Delta S + \Delta R_Z, \tag{16a}$$

$$\Delta T_Z = \Delta T - \frac{\Delta\bar{\delta}_G}{\alpha} + 1.49\Delta R_Z. \tag{16b}$$

The factor $\bar{\delta}_G$ is the vertex and box corrections to the muon decay constant, G_F [88], and $\Delta\bar{\delta}_G$ is the shift from its SM value, $\bar{\delta}_G = 0.0055 + \Delta\bar{\delta}_G$ [87]. The R_Z-parameter accounts for the difference between S and S_Z, and represents the running effect of the Z boson propagator corrections between $q^2 = m_Z^2$ and $q^2 = 0$ [1]. We define it as

$$R_Z \equiv -16\pi\left(\frac{1}{\bar{g}_Z^2(m_Z^2)} - \frac{1}{\bar{g}_Z^2(0)}\right), \tag{17}$$

and ΔR_Z denotes the shift from the value of R_Z at the SM reference point, 1.1879 [1]:

$$R_Z = 1.1879 + \Delta R_Z. \tag{18}$$

In this study, we use the W-boson properties, m_W and Γ_W, for the fit. Instead of ΔU, as the third oblique parameter we take $\Delta m_W = m_W - 80.365(\text{GeV})$ which is given as a function of $\Delta S, \Delta T, \Delta U, x_\alpha$ and $\Delta\bar{\delta}_G$, as [1]

$$\Delta m_W(\text{GeV}) = -0.288\Delta S + 0.418\Delta T + 0.337\Delta U - 0.0055x_\alpha - 0.126\frac{\Delta\bar{\delta}_G}{\alpha}. \tag{19}$$

We also parametrize the W-boson decay width, Γ_W. To do so, it is useful to introduce the parameter R_W which parametrizes the running of the W boson coupling $\bar{g}_W(q^2)$ between the zero momentum transfer and $q^2 = m_Z^2$, since the decay width is roughly given by

$$\Gamma_W = 3.3904 \times 10^{-1} m_W^3 G_F\left(1 + 8.478 \times 10^{-3} R_W + 0.00065x_s\right), \tag{20}$$

where, in analogy to Eq. (17), we define R_W by

$$R_W = -16\pi\left(\frac{1}{\bar{g}_W^2(m_Z^2)} - \frac{1}{\bar{g}_W^2(0)}\right), \tag{21}$$

and define ΔR_W as the shift from its value at the SM reference point:

$$R_W = 2.1940 + \Delta R_W. \tag{22}$$

The SM contributions to the oblique parameters, S_Z, T_Z, m_W and R_Z are given in Refs. [1, 89] as functions of m_t and $m_{H_{\text{SM}}}$. We update the parametrization as

$$(\Delta S_Z)_{\text{SM}} = 0.2217x_h - 0.1188x_h^2 + 0.0320x_h^3 - 0.0014x_t + 0.0005x_s, \tag{23a}$$

$$\begin{aligned}(\Delta T_Z)_{\text{SM}} = &-0.0995x_h - 0.2858x_h^2 + 0.1175x_h^3 + 0.0367x_t + 0.00026x_t^2 \\ &-0.0017x_hx_t - 0.0033x_s - 0.0001x_tx_s,\end{aligned} \tag{23b}$$

$$(\Delta m_W)_{\text{SM}} = -0.137x_h - 0.019x_h^2 + 0.018x_t - 0.005x_\alpha - 0.002x_s, \tag{23c}$$

$$(\Delta R_Z)_{\text{SM}} = -0.124\left\{\ln\left[1 + \left(\frac{26}{m_{H_{\text{SM}}}(\text{GeV})}\right)^2\right] - \ln\left[1 + \left(\frac{26}{100}\right)^2\right]\right\}, \tag{23d}$$

$$(\Delta R_W)_{\text{SM}} = -0.16\left\{\ln\left[1 + \left(\frac{23}{m_{H_{\text{SM}}}(\text{GeV})}\right)^2\right] - \ln\left[1 + \left(\frac{23}{100}\right)^2\right]\right\}. \tag{23e}$$

	C_{fV}	C_{fA}	$\delta^f_{\mathrm{Im}\,\kappa}$	$\Delta^f_{\mathrm{EW/QCD}}$ [GeV]
u	$3.1166 + 0.0030x_s$	$3.1377 + 0.00014x_t + 0.0041x_s$	0.0000146	−0.000113
d, s	$3.1167 + 0.0030x_s$	$3.0956 - 0.00015x_t + 0.0019x_s$	0.0000032	−0.000160
c	$3.1167 + 0.0030x_s$	$3.1369 + 0.00014x_t + 0.0043x_s$	0.0000146	−0.000113
b	$3.1185 + 0.0030x_s$	$3.0758 - 0.00015x_t + 0.0028x_s$	0.0000026	−0.000040
ν	1	1	0	0
e, μ	1	1	0.0000368	0
τ	1	0.9977	0.0000368	0

Table 4: The numerical values of the factors C_{fV}, C_{fA}, $\delta^f_{\mathrm{Im}\,\kappa}$ and $\Delta^f_{\mathrm{EW/QCD}}$ which appear in the expression for the partial widths of the Z boson.

The parameters x_t, x_h and x_s are defined as

$$x_t = \frac{m_t - 172\mathrm{GeV}}{3\mathrm{GeV}}, \qquad x_h = \frac{\ln(m_{H_{\mathrm{SM}}}/100\mathrm{GeV})}{\ln 10}, \qquad x_s = \frac{\hat{\alpha}_s(m_Z)_{5q} - 0.118}{0.003}, \tag{24}$$

so that their numerical values are expected to be less than unity. As for the vertex corrections, the shift $(\Delta g^b_{L,R})_{\mathrm{SM}}$ in the SM is given by

$$(\Delta g^b_L)_{\mathrm{SM}} = -0.000058x_h + 0.000128x_t, \tag{25a}$$
$$(\Delta g^b_R)_{\mathrm{SM}} = -0.000042x_h - 0.000025x_h^4, \tag{25b}$$

where the x_h^4 term in the equation for $(\Delta g^b_R)_{\mathrm{SM}}$ is purely from the result of the numerical fit.

Using the effective coupling g^f_α, the electroweak observables can be written in the following way. First, the Z-boson partial decay width into $f\bar{f}$ is,

$$\Gamma_f = \frac{G_F m_Z^3}{6\sqrt{2}\pi}\left[\left((g^f_V)^2 + \delta^f_{\mathrm{Im}\,\kappa}\right)C_{fV} + (g^f_A)^2 C_{fA}\right]\left(1 + \frac{3}{4}Q_f^2\frac{\hat{\alpha}(m_Z)}{\pi}\right) + \Delta^f_{\mathrm{EW/QCD}}\,. \tag{26}$$

The value of each correction factor is summarized in Table 4. C_{fV} and C_{fA} describe the corrections to the color factor in the vector and axial-vector currents, respectively, which have a dependence on α_s and m_t. The term $\delta^f_{\mathrm{Im}\,\kappa}$ represents the corrections from the imaginary part of loop-induced mixing of the photon and the Z boson. The term $\Delta^f_{\mathrm{EW/QCD}}$ is the non-factorizable mixed electroweak and QCD corrections [90], whose values in Table 4 have been copied from the second paper of Ref. [91]. Q_f is the electric charge of the fermion f in the normalization that $Q_f = -1$ for the electron.

As a check of our parametrization, in Fig. 4 we give a comparison of χ^2_{min} constructed from the fit for the first 15 observables in Table 5 together with $m_t, \Delta\alpha^{(5)}_{\mathrm{had}}(m_Z^2), \hat{\alpha}_s(m_Z)_{5q}$ as a function of $m_{H_{\mathrm{SM}}}$ by using `ZFITTER` [91] and that fitted by using our parametrization. Since our parametrization is designed so that it gives a good description only in the region $100\mathrm{GeV} \leq m_{H_{\mathrm{SM}}} \leq 1000$ GeV, we find that the agreement becomes worse for $m_{H_{\mathrm{SM}}} \lesssim 100$ GeV.

In Table 5, we show the electroweak observables used in the present analysis. The experimental values of the Z pole observables, including the correlations among errors that

	data	SM		without A_j	
LEP 1		best fit	pull	best fit	pull
line-shape & FB asym.:					
Γ_Z (GeV)	2.4952(23)	2.4958	-0.25	2.4963	-0.46
σ_h^0(nb)	41.540(37)	41.478	1.67	41.478	1.69
R_l	20.767(25)	20.743	0.98	20.746	0.82
$A_{\rm FB}^{0,l}$	0.01714(95)	0.01647	0.71	0.01690	0.26
τ polarization:					
$A_\tau(P_\tau)$	0.1465(32)	0.1482	-0.52	0.1501	-1.11
b and c quark results:					
R_b	0.21629(66)	0.21583	0.70	0.21581	0.72
R_c	0.1721(30)	0.1722	-0.05	0.1723	-0.05
$A_{\rm FB}^{0,b}$	0.0992(16)	0.1039	-2.92	—	—
$A_{\rm FB}^{0,c}$	0.0707(35)	0.0743	-1.02	—	—
jet charge asymmetry:					
$\sin^2\theta_{\rm eff}^{\rm lept}$	0.2324(12)	0.2314	0.85	—	—
SLC					
$A_{\rm LR}^0(A_e)$	0.1513(21)	0.1482	1.51	0.1501	0.58
A_b	0.923(20)	0.935	-0.58	—	—
A_c	0.670(27)	0.668	0.06	—	—
Tevatron + LEP 2					
m_W (GeV)	80.399(23)	80.376	0.99	80.400	-0.04
Γ_W (GeV)	2.085(42)	2.092	-0.16	2.093	-0.19
Numerical inputs					
m_Z (GeV)	91.1875(21)	—	—	—	—
$G_F(10^{-5}{\rm GeV}^{-2})$	1.16637(1)	—	—	—	—
Parameters					
$\Delta\alpha_{\rm had}^{(5)}(m_Z^2)$	0.02759(15)	0.02761	-0.14	0.02759	0.01
$\hat\alpha_s(m_Z)_{5q}$	0.1184(7)	0.1184	0.00	0.1184	0.06
m_t (GeV)	172.0(1.6)	172.3	-0.17	171.9	0.05
$m_{H_{\rm SM}}$ (GeV)	—	84.4	—	48.9	—
$\chi^2_{\rm min}$			17.49		5.35
d.o.f.			$18-4$		$13-4$

Table 5: The electroweak precision data, the SM best fit values and the pull factors. The SM predictions and the pull factors have been calculated by using `ZFITTER` [91] by varying m_t, $m_{H_{\rm SM}}$, $\hat\alpha_s(m_Z)_{5q}$ and $\Delta\alpha_{\rm had}^{(5)}(m_Z^2)$ as input parameters. The values of the observables are taken from Ref. [3], except that m_W, Γ_W, m_t and $\hat\alpha_s(m_Z)_{5q}$ are from Ref. [13], and $\Delta\alpha_{\rm had}^{(5)}(m_Z^2)$ is from Ref. [8]. The values of m_Z and G_F are fixed throughout the calculation. The correlation matrix elements of the Z line-shape parameters and those for the heavy-quark parameters are found in Ref. [3]. We also show the SM fit and the associated pull factors in the case where we do not use the jet asymmetry data, namely, $A_{\rm FB}^{0,b}$, $A_{\rm FB}^{0,c}$, $\sin^2\theta_{\rm eff}^{\rm lept}$, A_b and A_c.

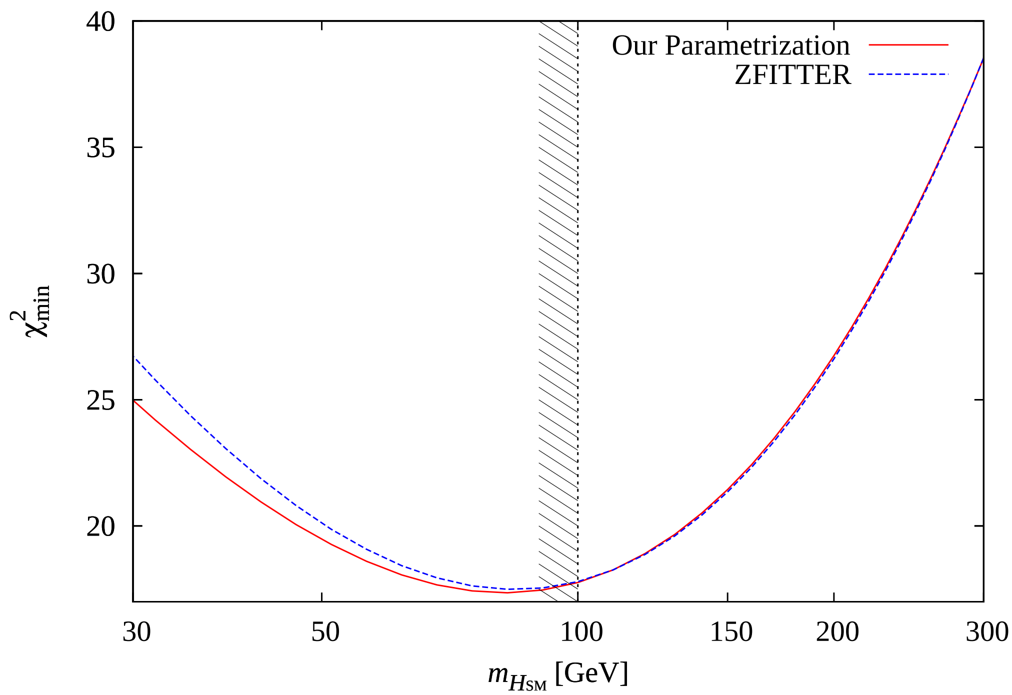

Figure 4: The comparison of $\chi^2_{\rm min}$ of the electroweak observables as a function of the SM Higgs boson mass $m_{H_{\rm SM}}$ fitted by using our parametrization (solid line) and by using the output of `ZFITTER` (dashed line). Our parametrization is valid for $m_{H_{\rm SM}} > 100$ GeV.

are not reproduced in Table 5, are taken from Ref. [3]. The values of m_W, Γ_W, m_t and $\hat{\alpha}_s(m_Z)_{5q}$ are taken from Ref. [13], and the value of $\Delta\alpha^{(5)}_{\rm had}(m_Z^2)$,

$$\Delta\alpha^{(5)}_{\rm had}(m_Z^2) = 0.02759 \pm 0.00015, \tag{27}$$

is from Ref. [8], in which the prediction Eq. (2) for the muon $g-2$ is found. In Table 5 we also show the SM best fit values calculated by using `ZFITTER` by varying m_t, $m_{H_{\rm SM}}$, $\hat{\alpha}_s(m_Z)$ and $\Delta\alpha^{(5)}_{\rm had}(m_Z^2)$ as the input parameters. m_Z and G_F are fixed at their central values throughout our analysis.

Here we consider two cases, the case using all data and the case without using the jet asymmetry data, namely, $A^{0,b}_{FB}$, $A^{0,c}_{FB}$, $\sin^2\theta^{\rm lept}_{\rm eff}$, A_b and A_c, because there is still theoretical uncertainty in the calculation of QCD corrections [57]. In the last two rows of Table 5, we show the values of $\chi^2_{\rm min}$ and degrees-of-freedom (d.o.f.), which is the number of used data minus the number of input parameters. From the fit and the value of $\chi^2_{\rm min}$, we can see that the SM with the light Higgs boson gives a good description of the data. If we remove the jet asymmetry data, a lighter Higgs boson is favored. Once the best fit parameters are fixed, the corresponding values for the observables can be calculated immediately, and these SM best fit values and the associated pull factors are also shown in Table 5.

4 The precision data and the MSSM

In this section, assuming that there is new physics which gives rise to finite corrections to ΔS_Z and ΔT_Z, we estimate the region of ΔS_Z and ΔT_Z favored by the Z-pole observables. Then, under the assumption that the new physics is the MSSM, we use the constraints from ΔS_Z and ΔT_Z to find the favored range of the MSSM parameters. Later in this section we use m_W as another observable to constrain the favored SUSY parameters. We conclude this section with the discussion of the case where we do not use the jet asymmetry data.

4.1 Oblique Corrections

In this subsection, we first identify the favored parameter range of ΔS_Z and ΔT_Z. The assumptions to compute the theoretical predictions are the following. The input free parameters from the new physics are taken to be ΔS_Z, ΔT_Z, and Δg_L^b. All the other vertex corrections Δg_α^f are neglected for simplicity. As for the SM parameters, we fix x_t and x_α at $x_t = x_\alpha = 0$ as a "reference point". Consequences from different choices of x_t and x_α can be easily drawn, as discussed later. We take the reference SM Higgs boson mass to be $m_{H_{\rm SM}} = 120$ GeV in this section. As for the other input SM parameter x_s, instead of fixing it at $x_s = 0$, we include it in the χ^2 function, and only after finding the minimum of the χ^2 function, we integrate out x_s.

Using the mean values, the errors and the correlation matrix of the observables in Ref. [3], we obtain

$$\left.\begin{aligned} \Delta S_Z &= 0.020 - 2.22\Delta g_L^b - 0.031 x_\alpha \pm 0.106 \\ \Delta T_Z &= 0.053 + 0.50\Delta g_L^b \pm 0.137 \end{aligned}\right\} \quad \rho_{\rm corr} = 0.91, \tag{28}$$

$$\Delta g_L^b = -0.00033 \pm 0.00082, \tag{29}$$

$$\chi^2_{\rm min} = 15.5, \tag{30}$$

where $\rho_{\rm corr}$ is the correlation between ΔS_Z and ΔT_Z. In Fig. 5, we show the contours for the 39% and the 90% confidence levels (CL) as shown in Eqs. (28), and also plot the SM prediction for $m_{H_{\rm SM}} = 120$GeV, $m_t = 172$GeV and $\Delta\alpha_{\rm had}^{(5)}(m_Z^2) = 0.0277$ as the big open circle at the origin. Although the ΔS_Z and ΔT_Z values which give the minimum χ^2 value are slightly different from the prediction at the SM reference point, these shifts are within the 1-σ error. We also illustrate how the SM reference point moves according to the change of m_t from 172GeV to 175GeV and to $m_t = 169$GeV, as the "ruler" toward the right end of the figure. As we can see, the SM prediction for ΔT_Z becomes larger for larger m_t, while ΔS_Z does not change very much because of the stronger dependence of ΔT_Z on m_t, see Eq. (23b). The dependence of the plot on $\Delta\alpha_{\rm had}^{(5)}(m_Z^2)$ is shown as another "ruler" at the bottom of the figure. For example, if $\Delta\alpha_{\rm had}^{(5)}(m_Z^2) - 0.0277 > 0$, then the origin moves to the right, and the agreement of the SM reference point to the data becomes better.

In Fig. 5, we also show separately the slepton, squark and ino contributions to ΔS_Z and ΔT_Z. In the figure we take $\tan\beta = 10$, but these SUSY contributions do not change very much for $10 \lesssim \tan\beta \lesssim 50$. The qualitative behaviors of those contributions on the ΔS_Z-ΔT_Z plane have been studied in Ref. [1].

In the figure, the contributions to ΔS_Z and ΔT_Z from the sum of three generations of squarks for the cases $m_{\tilde{Q}}$=300 GeV and 500 GeV without left-right mixing among the

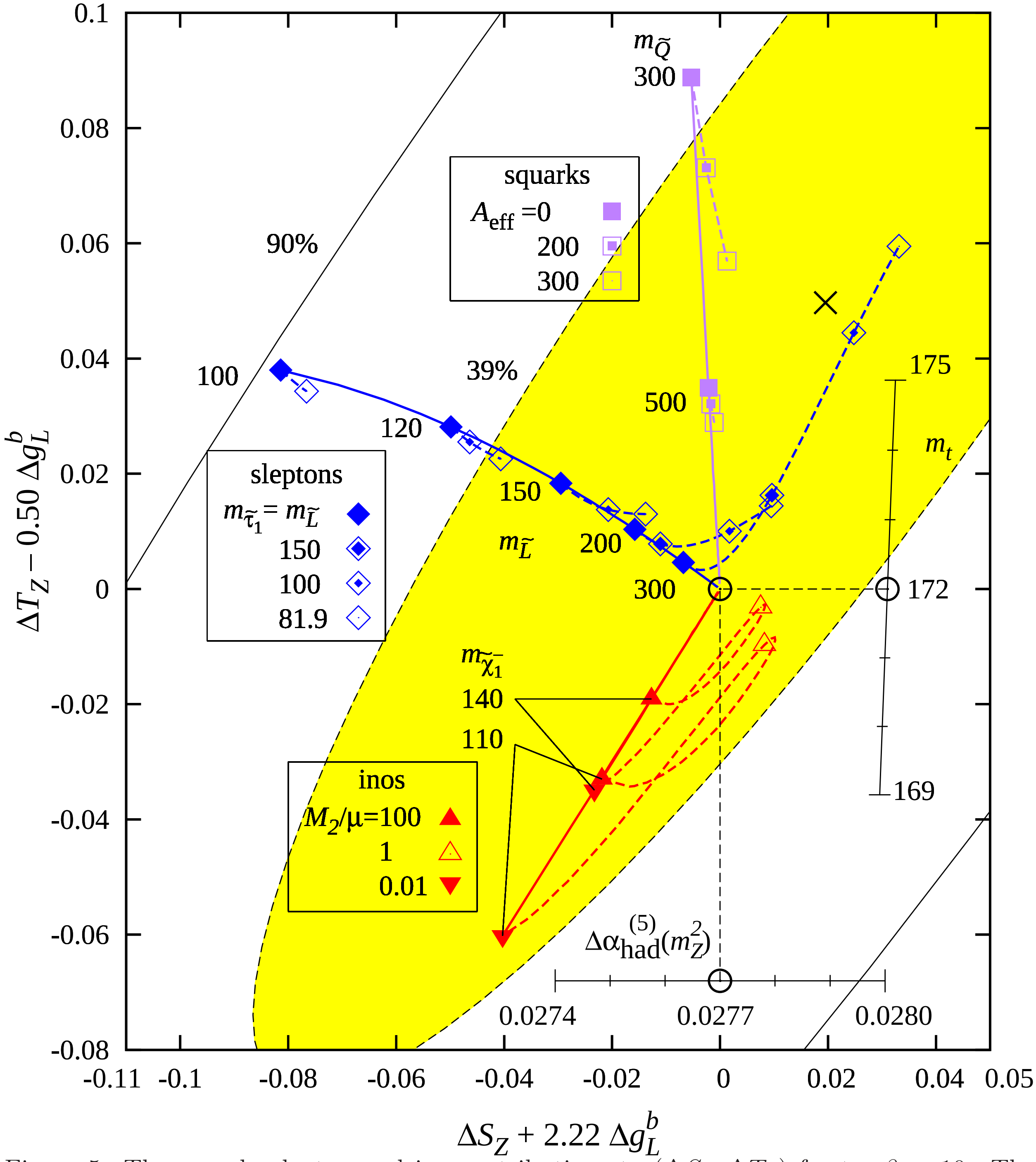

Figure 5: The squark, slepton and ino contributions to $(\Delta S_Z, \Delta T_Z)$ for $\tan\beta = 10$. The SUSY breaking scalar masses for the left-handed and right-handed squarks are assumed to be same, denoted by $m_{\tilde{Q}}$. The $\tilde{t}_L$-$\tilde{t}_R$ and $\tilde{b}_L$-$\tilde{b}_R$ mixings are controlled by $A_{\text{eff}} = A^t_{\text{eff}} = A^b_{\text{eff}}$. The left- and right-handed sleptons are also assumed to have a common SUSY breaking scalar mass $m_{\tilde{L}}$. The reference SM point, $(m_t, m_{H_{\text{SM}}}, \Delta\alpha^{(5)}_{\text{had}}(m_Z^2)) = (172\text{GeV}, 120\text{GeV}, 0.0277)$, is marked by the open circle at the origin of the plot. If a different value of m_t is chosen, then the origin would move according to the scale shown at the right-hand side. Similarly, if a different value of $\Delta\alpha^{(5)}_{\text{had}}(m_Z^2)$ is chosen, the origin would move according to the scale shown at the bottom.

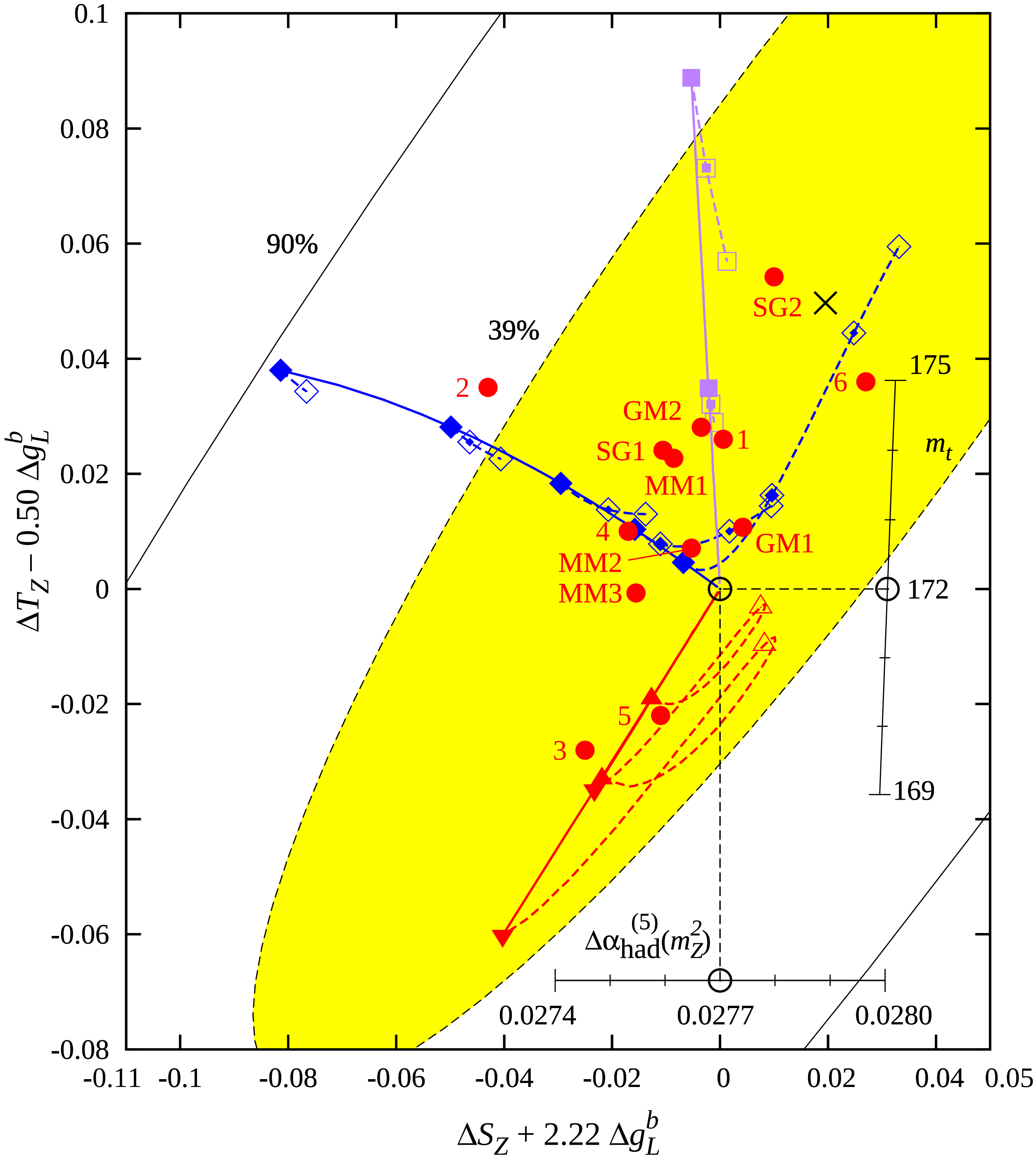

Figure 6: The predictions from our SUSY sample points, superposed on Fig. 5.

squarks are given as the filled squares. In the figure, we assume $m_{\tilde{Q}} = m_{\tilde{u}_R} = m_{\tilde{d}_R}$ for simplicity. The effects of the left-right mixing on these predictions are shown by the dashed lines starting from these squares. On each dashed line, the squark soft mass $m_{\tilde{Q}}$ is fixed at the same value, and along the dashed line, the parameter $A_{\rm eff}$ which controls the left-right mixing is varied from 0 to 300 GeV. (The definition of $A_{\rm eff}$ is the same as in Ref. [1][5].) The predictions for $A_{\rm eff} = 200$ GeV and 300 GeV are shown by the different squares on the dashed lines.

Similarly, the contributions to ΔS_Z and ΔT_Z from the sum of three generations of sleptons in the cases without left-right mixing are given by the filled diamonds labeled as $m_{\tilde{L}} = 100$, 120, . . ., 300 GeV. In the figure, for simplicity, we assume $m_{\tilde{L}} = m_{\tilde{E}}$, similarly to the squark case. Attached to these diamonds are the dashed lines which show the effects of the left-right mixing on these predictions. On each dashed line, the slepton soft mass $m_{\tilde{L}}$ is fixed at the same value, and the size of the left-right mixing is varied by using the lighter stau mass as the measure of the left-right mixing. In the figure, the cases where the lighter stau masses are 150, 100 and 81.9 GeV are shown by the different diamonds.

In Fig. 5, the ino contributions are also shown. The filled upward triangles are the predictions for the cases where the lighter chargino masses are 110 GeV and 140 GeV, respectively, in the Higgsino-like chargino cases with the ratio M_2/μ fixed at 100. On each dashed line the lighter chargino mass is fixed at the same value, while the ratio M_2/μ is varied from 100 to 0.01 along the dashed line.

The contributions to ΔS_Z from the squarks and sleptons can be understood as follows [1]. The ΔS_Z-parameter is defined as the sum of ΔS and ΔR_Z. When the left-right mixings of the sfermions are negligible, to one-loop order, ΔS receives contributions from left-handed sfermions, and is proportional to the hypercharge Y_f of the sfermion $\tilde{f}$ in the loop. The sign of the hypercharge is opposite between the left-handed squarks ($Y_{q_L} = +1/6$) and the left-handed sleptons ($Y_{\ell_L} = -1/2$), and this determines the sign of ΔS_Z in the limit of no left-right mixing. On the other hand, the sign of ΔR_Z-parameter is always negative for both squarks and sleptons contributions [1], and it adds up with ΔS constructively for sleptons while destructively for squarks. This is why ΔS_Z is negative for the sleptons and almost zero for the squarks.

The ΔT_Z-parameter is also defined as a linear combination of ΔT and ΔR_Z with small corrections from $\overline{\delta}_G - 0.0055$. As mentioned above, ΔR_Z is negative, but its magnitude for the sfermions is tiny compared to the contribution to ΔT [1].

To discuss the contributions to the ΔT-parameter from the sfermion sector, it is useful to separate three cases depending on the size of the left-right mixing of the sfermion: cases without the left-right mixing, with small left-right mixing and with large left-right mixing. First, in the case without left-right mixing, the contributions from the third generation

[5] For completeness, the definition of $A_{\rm eff}$ is as follows: the left-right mixing elements of the stop and the sbottom mass-squared matrices are given by $m_t(A_t - \mu/\tan\beta)$ and $m_b(A_b - \mu\tan\beta)$, respectively. (We are neglecting possible CP-violating phases for μ, A_t and A_b for simplicity.) We define $A^t_{\rm eff}$ and $A^b_{\rm eff}$ so that these left-right mixing elements are equal to $m_t A^t_{\rm eff}$ and $m_b A^b_{\rm eff}$, respectively: $A^t_{\rm eff} \equiv A_t - \mu/\tan\beta, A^b_{\rm eff} \equiv A_b - \mu\tan\beta$. In this paper, for simplicity we only consider the case $A^t_{\rm eff} = A^b_{\rm eff}$, and denote this common value by $A_{\rm eff}$.

squarks can be written as

$$(\Delta T)_{\tilde{t}_L\text{-}\tilde{b}_L} = \frac{G_F C_q}{12\sqrt{2}\pi^2\alpha} \frac{(m_{\tilde{t}_L}^2 - m_{\tilde{b}_L}^2)^2}{m_{\tilde{t}_L}^2 + m_{\tilde{b}_L}^2} \left[1 + \mathcal{O}\left(\left(\frac{(m_{\tilde{t}_L}^2 - m_{\tilde{b}_L}^2)^2}{m_{\tilde{t}_L}^2 + m_{\tilde{b}_L}^2} \right)^2 \right) \right], \tag{31}$$

where C_q is the color factor ($C_q = 3$ for the squarks) and we take the limit where the squarks are heavy compared to m_t. The slepton contribution can be obtained by the obvious replacements $C_q \to 1$, $\tilde{t}_L \to \tilde{\nu}$ and $\tilde{b}_L \to \tilde{e}_L$. Second, when left-right mixing is small enough, the T-parameter decreases as $A_{\rm eff}$ increases, as studied in Ref. [1]. Third, when in the limit that left-right mixing is large, the T-parameter increases as $A_{\rm eff}$ increases [72]. The behavior of the stau contribution to ΔT_Z interpolates the above two limits.

The ino contributions are small in general once we impose the experimental constraint from the direct searches on the lightest chargino mass, unless the ino masses are close to the experimental bounds. When inos are light, the contributions to ΔR_Z can be sizable, which make negative contributions to S_Z and T_Z [1]. In Fig. 5, we show the cases $m_{\tilde{\chi}_1^-} \geq 110$GeV for $M_2/\mu = 0.01, 1$ and 100. For the cases $M_2/\mu = 0.01$ and 100, the predicted trajectories for $(\Delta S_Z, \Delta T_Z)$ overlap on the line $\Delta T_Z = 1.49\Delta S_Z$. This can be understood in the following way. Since the wino mass parameter M_2 and the Higgsino mass parameter μ do not break the $SU(2)_L \times U(1)_Y$ symmetry, the contribution from the ino sector to the S- and T-parameters can only come from the off-diagonal elements of the ino mass matrices. When $M_2/\mu = 0.01$ or 100, the mixing of the ino mass matrices are suppressed by $m_Z^2/(M_2^2 - \mu^2)$, which is small once we impose $m_{\tilde{\chi}_1^-} \geq 110$GeV and the strong hierarchy between M_2 and μ. Hence for these hierarchical cases, the contributions to ΔS_Z and ΔT_Z only come from ΔR_Z, namely, $\Delta S_Z = \Delta R_Z$ and $\Delta T_Z = 1.49\Delta R_Z$, which makes the trajectories on Fig. 5 overlap.

In Fig. 6, we plot our SUSY sample points on the same frame as that of Fig. 5.

In the cases of the six MSSM sample points, we can ignore the squark contributions because we set all the squark masses to be 2 TeV. So, almost all the MSSM scenarios are put near the slepton lines or ino lines. Only the sample point 1 is apart from both lines, because it has a sizable contribution from $\Delta\bar{\delta}_G$ to ΔT_Z by 0.036. Although it has the slepton contribution at $m_{\tilde{E}} = 300$GeV with small mass splitting and the ino contribution at $M_2/\mu = 0.75$ and $m_{\tilde{\chi}_1^-} = 115$GeV, these contribution are almost canceled out. The sample point 2 has a quite large contribution from slepton, because it has light sleptons. And it shifts above the solid line which shows the slepton contribution without the left-right mixing case due to the $\Delta\bar{\delta}_G$ contribution to ΔT_Z by 0.015. The sample points 3 and 5 are characteristic in the ino contribution, because of a light chargino mass, $m_{\tilde{\chi}_1^-} \sim 150$GeV, and a small M_2/μ ratio, $M_2/\mu = 0.19$. In particular, the sample point 5 has essentially only ino contribution because of heavy sleptons, ~ 800GeV. On the other hand, the sample point 3 has a non-negligible slepton contribution ($m_{\tilde{E}} \sim 200$GeV) compared to the sample point 5, and a small contribution from $\Delta\bar{\delta}_G$ of -0.010 to ΔT_Z. The sample point 4 is determined almost only by slepton contribution from $m_{\tilde{E}} = 150$GeV and $m_{\tilde{\tau}_1} \sim 100$GeV. The sample point 6 is an interesting point, because it is the case of large SUSY breaking mass, $m_{\tilde{E}} = 300$GeV with a light stau, $m_{\tilde{\tau}_1} = 144$GeV. In this parameter region ΔT increase as $A_{\rm eff}$ or squared mass difference increase.

As for the predictions from the selected scenario points, for all the selected model points except MM3, the ino contributions are negligible because there $m_{\tilde{\chi}_1^-} \geq 200$GeV. The SG2

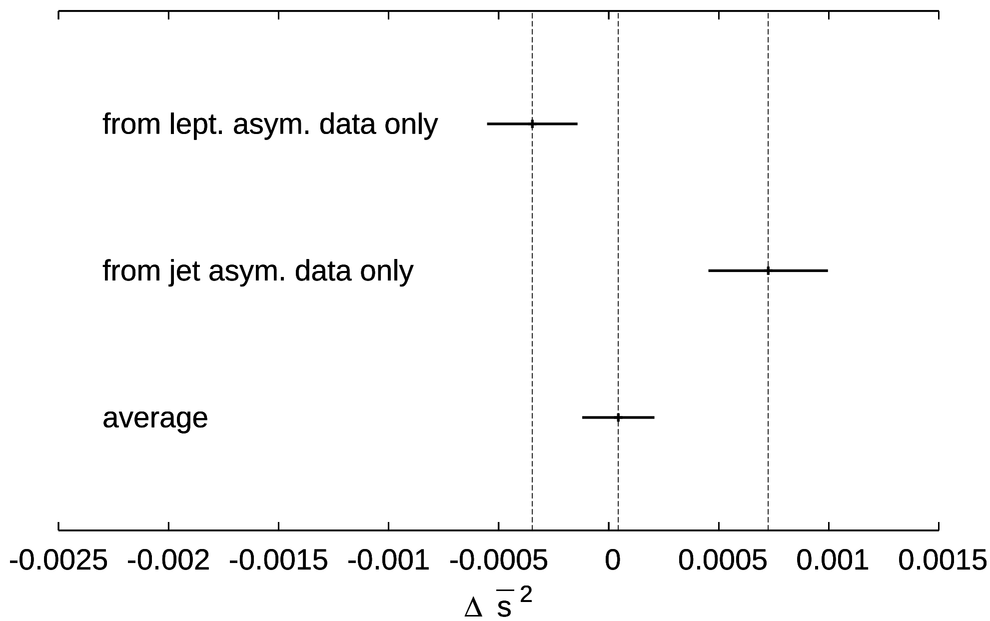

Figure 7: The favored ranges of $\Delta\bar{s}^2$ from the leptonic and the jet asymmetry data. Also shown is the favored value for the case where we combine all the leptonic and the jet asymmetry data.

scenario gives the largest contribution to ΔT_Z. This contribution mainly comes from slepton with a large $m_{\tilde{E}}$ with a large squared mass splitting, and the contributions from the other sectors are negligible because the squark masses are more than 1 TeV. The GM2 and MM2 scenarios also have heavy squarks, and in the large SUSY breaking mass with light stau region, $(m_{\tilde{E}}, m_{\tilde{\tau}_1}) = (250\mathrm{GeV}, 120\mathrm{GeV})$ and $(245\mathrm{GeV}, 104\mathrm{GeV})$, respectively. The SG1 and MM1 scenarios have similar parameters, and are located at almost the same place in the ΔS_Z-ΔT_Z plane. At the GM1 point, we can neglect the slepton contribution because of large mass, ~ 440GeV, and it has the contribution from squarks at $m_{\tilde{q}} \sim 800$GeV and the $\Delta\bar{\delta}_G$ contribution, 0.014.

In Figs. 5 and 6, we do not show the contributions from Higgs bosons, which are known to be small for $m_h > 115$ GeV [1]. In fact, for our selected scenarios SG1,...,MM3, the contributions from the Higgs sector is $0 < \Delta S_Z \lesssim 0.004$ and $-0.003 \lesssim \Delta T_Z < 0$.

4.2 Data without Jet Asymmetry and Oblique Corrections

It may be worth repeating the above analysis after excluding the jet asymmetry data from the input Z-pole precision observables.

The pull factor in Table 5 shows that the data of b-jet forward-backward asymmetry differ from the theoretical expectation by roughly three standard-deviations. This can be seen more clearly if we look into the favored region of $\Delta\bar{s}^2$ separately from leptonic asymmetry and jet asymmetry. The results are summarized in Fig. 7. From the figure we can see that the value of $\Delta\bar{s}^2$ determined from the leptonic asymmetry data ($A_{\mathrm{FB}}^{0,l}$, $A_\tau(P_\tau)$, A_{LR}^0) does not agree very well with that determined from the jet asymmetry data ($A_{\mathrm{FB}}^{0,b}$, $A_{\mathrm{FB}}^{0,c}$, $\sin^2\theta_{\mathrm{eff}}^{\mathrm{lept}}$, A_b, A_c).

In fact, the values for $\Delta\bar{s}^2$ for these cases are separately

$$\Delta\bar{s}^2 = -0.00035 \pm 0.00021 \quad \text{(lepton only)}, \tag{32}$$

$$\Delta\bar{s}^2 = +0.00072 \pm 0.00027 \quad \text{(jet only)}. \tag{33}$$

The fit for the lepton asymmetry data gives $\chi^2_{\rm min}/\text{d.o.f.} = 1.64/(3-1)$, or the probability 44%. On the other hand, the fit for the jet asymmetry gives $0.39/(5-1)$, or the probability 98%. The values in Eqs. (32) and (33) differ by 3.1 σ. If we average the two values blindly, we obtain

$$\Delta\bar{s}^2 = 0.000044 \pm 0.00016 \quad \text{(all asymmetry data)}, \tag{34}$$

with $\chi^2_{\rm min} = 9.9$. This implies that the asymmetry data agree well within the leptonic data and the jet data separately, but not very well between the two sets. Although the same result (34) is obtained by averaging all the asymmetry data at once, with $\chi^2_{\rm min}/\text{d.o.f.} = 11.9/(8-1)$, we feel that this low value of $\chi^2_{\rm min}/\text{d.o.f.}$ is an artifact caused by using data with large statistical errors. Since we take seriously the possible deviation from the SM in the muon $g-2$, we would like to take the difference between (32) and (33) seriously.

Recently, the jet angular distribution in e^+e^- annihilation has been re-examined [57] in the framework of soft-collinear effective theory [92] and a local current-three-parton ($q\bar{q}g$) operator which contributes to the reduction of the forward-backward asymmetry has been identified, and the associated parton shower (jet function) has been obtained in the NLL approximation of massless QCD. Although the quantitative effect estimated in Ref. [57] reduces the discrepancy between the quark and lepton measurements only slightly, the observation suggests that we may need to develop a parton shower program which is capable of simulating the jet angular distribution with the accuracy matching that of the precision measurements. Until the data can be re-analyzed by using such advanced tools, it may be worthwhile to examine consequences of dropping the constraints from all the jet asymmetry measurements.

When we leave out the data for $A_{FB}^{0,b}$, $A_{FB}^{0,c}$, $\sin^2\theta_{\rm eff}^{\rm lept}$, A_b and A_c, the favored region becomes

$$\left.\begin{array}{rl} \Delta S_Z = & -0.109 + 1.50\Delta g_L^b - 0.031 x_\alpha \pm 0.113 \\ \Delta T_Z = & 0.024 + 1.24\Delta g_L^b \pm 0.137 \end{array}\right\} \quad \rho_{\rm corr} = 0.87, \tag{35}$$

and the value of the minimum of χ^2 is

$$\chi^2_{\rm min} = 4.7 + \left(\frac{\Delta g_L^b + 0.00058}{0.00083}\right)^2. \tag{36}$$

As shown in Fig. 8, we find that the favored region has been shifted to the negative ΔS_Z direction. We also overlay the MSSM predictions already discussed in Fig. 6. We find that the favored region can be reached by relatively light ($\sim 100-120$GeV) sleptons. It is interesting to note that these light sleptons can explain the muon $g-2$ anomaly naturally.

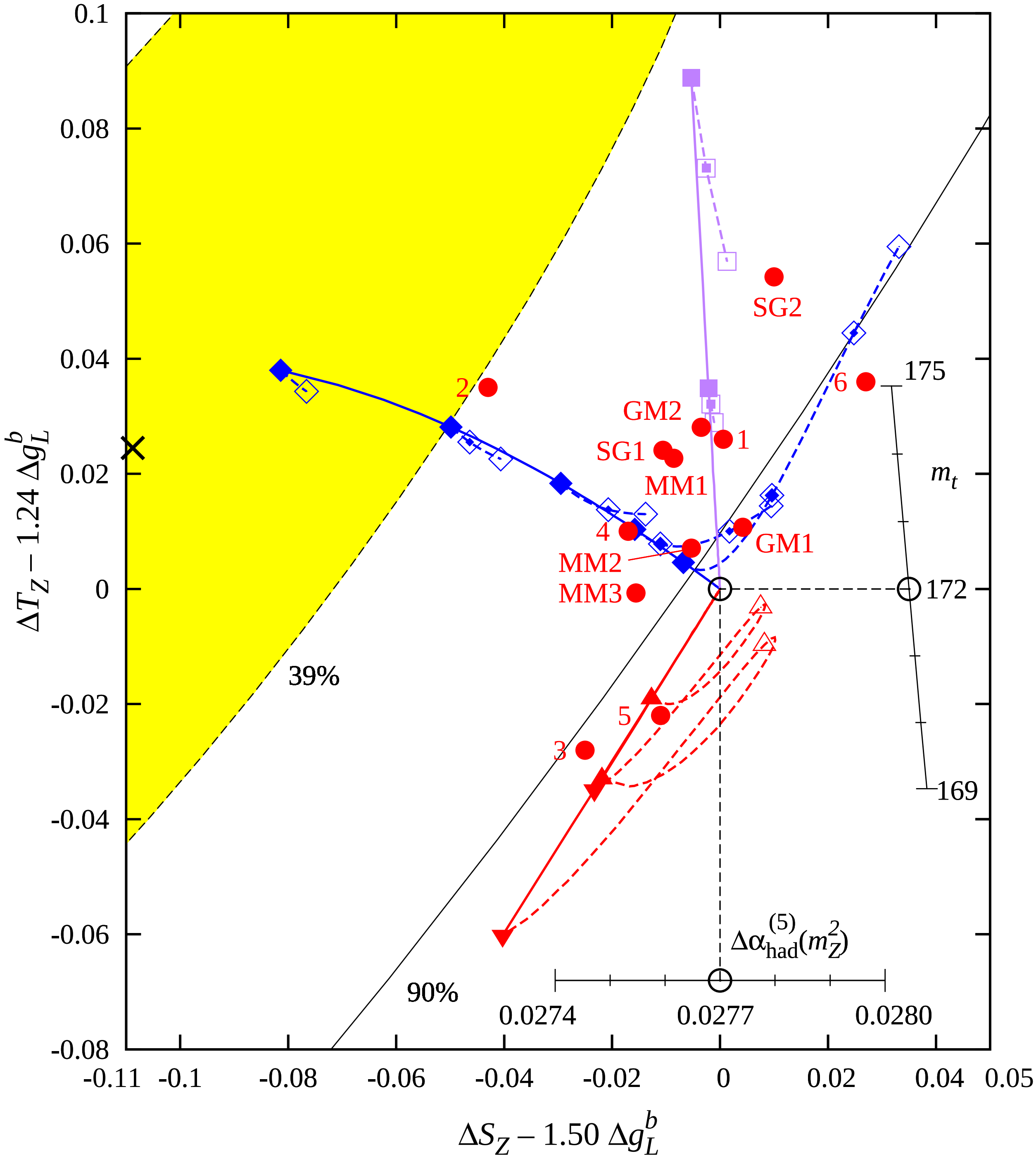

Figure 8: The same figure as Fig. 6 except that we omitted the jet asymmetry data.

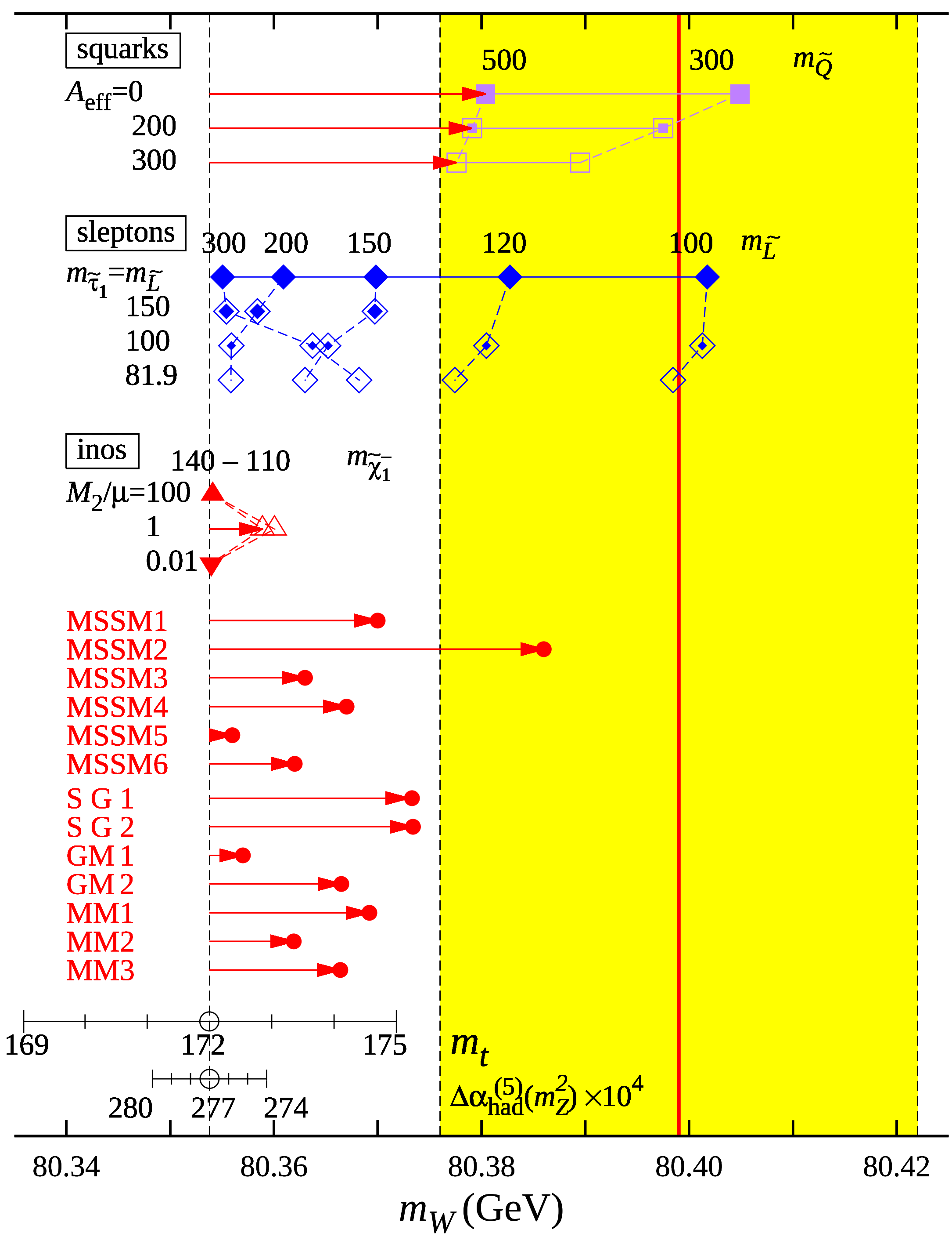

Figure 9: The MSSM predictions for the W boson mass from the squark, slepton and ino sectors, and from the MSSM sample points. The vertical dashed line at $m_W = 80.354$ GeV is the SM prediction for the SM reference point, $(m_t, m_{H_{\rm SM}}, \Delta\alpha^{(5)}_{\rm had}(m_Z^2)) = (172\text{GeV}, 120\text{GeV}, 0.0277)$. The dependences of the SM prediction on m_t and $\Delta\alpha^{(5)}_{\rm had}(m_Z^2)$ are shown at the bottom. Also shown as the red/solid line and the yellow/shaded band are the experimental mean and the 1-σ uncertainty, respectively.

4.3 m_W in the MSSM

In our framework, the W boson mass is a quantity which can be calculated from input parameters. The predicted SM value of m_W for our SM reference point $(m_t, m_{H_{\rm SM}}, \Delta\alpha^{(5)}_{\rm had}(m_Z^2)) = (172\text{GeV}, 120\text{GeV}, 0.0277)$ is given in Fig. 9 as the vertical dashed line at $m_W = 80.354$ GeV. We see that it is away from the experimental result, whose mean is shown as the solid vertical line at $m_W = 80.399$ GeV together with its uncertainty shown as the band, roughly at 2-σ level. At the bottom of the figure we show the dependences of the SM prediction for m_W on m_t and $\Delta\alpha^{(5)}_{\rm had}(m_Z^2)$. When m_t becomes larger the prediction also becomes larger because Δm_W has a rather strong dependence on ΔT, see Eq. (19), and ΔT has also positive dependence on m_t as Eq. (23b). The dependence on $\Delta\alpha^{(5)}_{\rm had}(m_Z^2)$ is not as strong as on m_t, but is not negligible.

In Fig. 9, we also show the individual contributions to the W boson mass from each sector in the MSSM. In the figure we take $\tan\beta = 10$, but these SUSY contributions do not change very much for $10 \lesssim \tan\beta \lesssim 50$. The squark and slepton contributions to m_W are examined for the same parameter space in Fig. 6. They make the fit to the m_W data better than the SM. The sfermion contributions shift m_W into the 1-σ favored range, when $m_{\tilde{Q}} \lesssim 500$GeV or when $m_{\tilde{L}} \lesssim 140$GeV. These improvements mainly come from the ΔT and the ΔS terms in Eq. (19) for the squark and the slepton, respectively. As for the dependence on the $A_{\rm eff}$ term, in the case of squarks, a larger left-right mixing makes the correction to m_W smaller. This can also be explained by the dependence of ΔT on $A_{\rm eff}$, as already seen in Fig. 6. Similarly, also for the sleptons, when the left-right mixing is not extremely large, the larger $A_{\rm eff}$ predicts smaller Δm_W. However, when the left-right mixing is extremely large, the contribution to ΔT becomes large, as already discussed, which also makes Δm_W large, as seen for $(m_L, m_{\tilde{\tau}_1}) = (300, \sim 100)$ GeV in Fig. 9.

The ino contributions to m_W are examined for $110\text{GeV} \le m_{\tilde{\chi}_1^-} \le 140\text{GeV}$ and for $M_2/\mu = 0.01, 1$ and 100. They are relatively small compared to the squarks and sleptons. Among the three cases, only the mixed case ($M_2/\mu = 1$) gives a sizable correction to m_W. This can also be understood from the discussion on ΔS and ΔT in Section 4.1.

In Fig. 9 we also show the predictions from the sample SUSY parameter sets. We see that for all the SUSY sample points the predicted values for m_W are improved compared to the SM reference point. Among them, when there is a light slepton, like at MSSM2, MSSM4 and MSSM6, the improvement is large since the slepton contributions are larger than inos for similar masses. In particular, at MSSM2, where both the sleptons are light, the improvement is most effective.

Also for the predictions from the selected SUSY breaking scenarios, SG1,...,MM3, the points with light sleptons make large contributions to m_W, like SG1, GM2, MM1–3. At SG2, the left-right mixing of the stau makes the contribution large. At GM1, since there are no light sleptons, the contribution is small.

In Fig. 9 we do not show the dependence on the Higgs sector since it is known to be small [1]. For our selected scenarios SG1,...,MM3, the contributions from the Higgs sector is $-3\text{MeV} \lesssim \Delta m_W < 0$, which is negligible compared to the experimental uncertainty.

4.4 Γ_W in the MSSM

The SUSY corrections to the W boson decay width, Γ_W, can also be calculated once the SUSY parameters are fixed. The SM prediction for $(m_{H_{\rm SM}}, m_t) = (120, 172)$ GeV is $\Gamma_W = 2.090$ GeV, which is consistent with the experimental value, $\Gamma_W = 2.085 \pm 0.042$ GeV [13]. Compared to the experimental uncertainty, the SUSY corrections to Γ_W are very small (~ 0.001 GeV) for our sample SUSY parameters, and we find that Γ_W is not as useful as other EW precision parameters to constrain SUSY contributions.

4.5 Summary of Electroweak Observables

In Tables 6 and 7 we summarize the values of the SUSY contribution to the oblique parameters and the electroweak observables for our sample parameters. From the tables, we see that for our sample parameters the SUSY corrections are small in general since for those points the SUSY particles are at the range of a few hundred GeV or heavier.

Next, if we look into the observables in Tables 6 and 7, we see that the observables like A_c and $\sin^2\theta_{\rm eff}^{\rm lept}$ do not depend on SUSY parameters very much compared to the experimental accuracy. We also see that some jet asymmetry observables like $A_{\rm FB}^{0,b}$, $A_{\rm FB}^{0,c}$ and A_b do not agree between experiment and SM, which SUSY contributions cannot improve very much, as is well known.

We also give $\chi^2_{\rm min}$ for the cases where (i) all the data are used, (ii) only $A_{\rm FB}^{0,b}$ is excluded, (iii) the jet asymmetry data (data with $*$ in the tables) are excluded. We see that the values of $\chi^2_{\rm min}$ show sizable changes between the cases (i) and (ii), but not very much between (ii) and (iii). This may suggest that $A_{\rm FB}^{0,b}$ is the main source of the deviation of the SM from the data.

In Tables 6 and 7 we also give the SUSY contribution to the shift Δm_W. Since the shift can be written in terms of the oblique parameters by Eq. (19), we can calculate the shift also from the values of ΔS, ΔT, and so on in Tables 6 and 7. Since for our sample points ΔT is larger than ΔS, ΔU and $-\Delta\bar{\delta}_G/\alpha$, ΔT gives the main contribution to Δm_W. In those sample points with larger ΔT, such as SG1 and SG2, the predicted shift Δm_W is larger, which makes the fit of m_W better. Similarly, for those point with smaller ΔT, such as GM1 and MM2, the shift Δm_W is small, which makes the total χ^2 worse.

The SUSY contribution to Γ_W is small compared to the experimental accuracy, as seen from Tables 6 and 7. We conclude that it is not very useful to constrain SUSY contributions.

In this paper, we do not consider the SUSY non-oblique corrections other than $\Delta\bar{\delta}_G$. In the MSSM we expect that the corrections to the Z-b-$\bar{b}$ vertex is the largest among vertex corrections. We find that the SUSY contributions to $\Delta g^b_{L/R}$ are at most of the order of 10^{-4}, which is far smaller compared to the oblique corrections.

	data	SM	MSSM1	MSSM2	MSSM3	MSSM4	MSSM5	MSSM6
ΔS			0.033	-0.025	-0.001	-0.010	0.009	0.029
ΔT			0.040	0.048	0.016	0.023	0.005	0.038
ΔR_Z			-0.032	-0.017	-0.023	-0.007	-0.020	-0.002
Δm_W (GeV)			0.017	0.032	0.009	0.013	0.002	0.009
Γ_Z (GeV)	2.4952(23)	2.4948	2.4954	2.4960	2.4945	2.4952	2.4943	2.4950
σ_h^0 (nb)	41.540(37)	41.481	41.494	41.477	41.488	41.481	41.486	41.482
R_l	20.767(25)	20.737	20.734	20.745	20.731	20.739	20.733	20.735
$A_{\rm FB}^{0,l}$	0.01714(95)	0.01613	0.01626	0.01651	0.01622	0.01628	0.01614	0.01611
R_b	0.21629(66)	0.21585	0.21587	0.21586	0.21586	0.21585	0.21578	0.21578
R_c	0.1721(30)	0.1722	0.1722	0.1722	0.1722	0.1722	0.1722	0.1722
$*$ $A_{\rm FB}^{0,b}$	0.0992(16)	0.1028	0.1032	0.104	0.1031	0.1033	0.1029	0.1028
$*$ $A_{\rm FB}^{0,c}$	0.0707(35)	0.0735	0.0738	0.0744	0.0736	0.0738	0.0734	0.0734
$*$ $\sin^2\theta_{\rm eff}^{\rm lept}$	0.2324(12)	0.2316	0.2315	0.2314	0.2315	0.2315	0.2316	0.2316
$*$ A_b	0.923(20)	0.935	0.9347	0.9348	0.9346	0.9347	0.9354	0.9354
$*$ A_c	0.670(27)	0.668	0.668	0.669	0.668	0.668	0.668	0.668
$A_\tau(P_\tau)$	0.1465(32)	0.1467	0.1473	0.1483	0.1471	0.1473	0.1467	0.1466
$A_{\rm LR}^0(A_e)$	0.1513(21)	0.1467	0.1473	0.1483	0.1471	0.1473	0.1467	0.1466
m_W (GeV)	80.399(23)	80.354	80.370	80.386	80.363	80.367	80.356	80.362
Γ_W (GeV)	2.085(42)	2.090	2.092	2.093	2.091	2.091	2.091	2.091
$\chi^2_{\rm EW}$ (all)		20.61	18.16	18.37	20.07	19.21	21.74	20.39
$\chi^2_{\rm EW}$ (excl. $A_{\rm FB}^{0,b}$)		16.32	12.76	10.59	15.08	13.71	17.26	16.11
$\chi^2_{\rm EW}$ (excl. $*$)		14.83	11.02	8.30	13.43	11.94	15.72	14.61

Table 6: The breakdown of the radiative corrections at our SUSY sample points MSSM1 – MSSM 6. In the column labeled as "SM", the values for the SM reference point $(m_t, m_{H_{\rm SM}}, \Delta\alpha_{\rm had}^{(5)}(m_Z^2)) = (172{\rm GeV}, 120{\rm GeV}, 0.0277)$ are given. The values for the SUSY corrections ΔS, ΔT, ΔR_Z and Δm_W are the deviations from this SM reference point.

	SG1	SG2	GM1	GM2	MM1	MM2	MM3
ΔS	0.008	0.012	0.009	0.006	0.003	0.005	0.003
ΔT	0.044	0.054	0.011	0.028	0.034	0.019	0.027
ΔR_Z	-0.019	-0.002	-0.005	-0.009	-0.011	-0.011	-0.019
Δm_W (GeV)	0.019	0.020	0.003	0.013	0.015	0.008	0.013
Γ_Z (GeV)	2.4958	2.4957	2.4948	2.4955	2.4956	2.4952	2.4952
σ_h^0 (nb)	41.486	41.484	41.485	41.483	41.483	41.485	41.486
R_l	20.738	20.734	20.734	20.739	20.739	20.736	20.736
$A_{\mathrm{FB}}^{0,l}$	0.01631	0.01630	0.01615	0.01626	0.01629	0.01620	0.01627
R_b	0.21589	0.21569	0.21575	0.21588	0.21588	0.21587	0.21588
R_c	0.1722	0.1723	0.1722	0.1722	0.1722	0.1722	0.1722
$*$ $A_{\mathrm{FB}}^{0,b}$	0.1034	0.1035	0.1030	0.1032	0.1033	0.1030	0.1032
$*$ $A_{\mathrm{FB}}^{0,c}$	0.0739	0.0739	0.0735	0.0738	0.0738	0.0736	0.0738
$*$ $\sin^2\theta_{\mathrm{eff}}^{\mathrm{lept}}$	0.2315	0.2315	0.2316	0.2315	0.2315	0.2315	0.2315
$*$ A_b	0.935	0.936	0.936	0.935	0.935	0.935	0.935
$*$ A_c	0.668	0.668	0.668	0.668	0.668	0.668	0.668
$A_\tau(P_\tau)$	0.1475	0.1474	0.1468	0.1472	0.1474	0.1470	0.1473
$A_{LR}^0(A_e)$	0.1475	0.1474	0.1468	0.1472	0.1474	0.1470	0.1473
m_W (GeV)	80.373	80.373	80.357	80.366	80.369	80.362	80.366
Γ_W (GeV)	2.092	2.091	2.090	2.091	2.091	2.091	2.092
χ^2_{EW} (all)	18.08	19.38	21.44	18.97	18.65	19.70	19.05
χ^2_{EW} (excl. $A_{\mathrm{FB}}^{0,b}$)	12.19	13.23	16.69	13.53	13.01	14.85	13.61
χ^2_{EW} (excl. $*$)	10.34	11.30	15.08	11.78	11.22	13.24	11.86

Table 7: The breakdown of the radiative corrections at our sample points in the selected SUSY models.

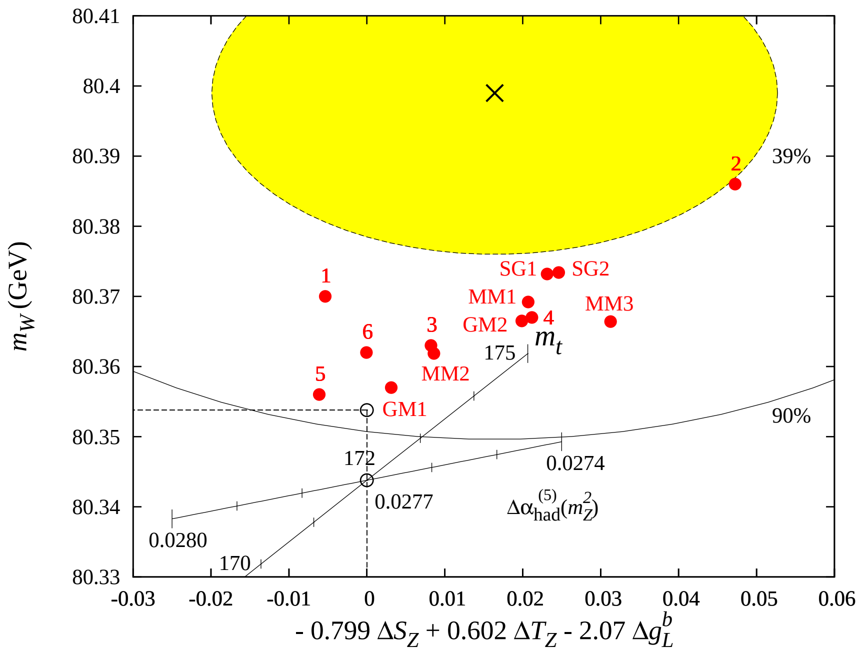

Figure 10: The favored region in the plane of the most experimentally constrained linear combination of ΔS_Z and ΔT_Z versus m_W. The inner/outer ellipses stand for the 39%/90% CL favored regions. The upper open circle is the SM prediction for $(m_t, m_{H_{\rm SM}}, \Delta\alpha_{\rm had}^{(5)}(m_Z^2)) = (172\text{GeV}, 120\text{GeV}, 0.0277)$. Also shown as the red/filled blobs are the predictions of our sample SUSY models. The lines with ticks around the lower open circle are the "rulers" to show how the SM prediction, and hence all the SUSY model prediction points as well, shifts when more accurate data on m_t and $\Delta\alpha_{\rm had}^{(5)}(m_Z^2)$ are available.

5 Preferred parameters in a few SUSY breaking models

In the previous section, we have studied the constraints from the EW precision data on ΔS_Z, ΔT_Z, and m_W. In Figs. 6 and 8, the constraints on ΔS_Z and ΔT_Z are shown by the favored region of an elliptic shape with a strong positive correlation. This means that the linear combination of ΔS_Z and ΔT_Z along the minor axis of the ellipse is constrained much stronger than the orthogonal combination along the major axis. We also note that this combination along the minor axis direction is strongly affected by the removal of the jet asymmetry constraints. In this section, we show the constraints on our $g-2$ favored SUSY models from the electroweak precision measurements in the plane of this strongly constrained combination and m_W, as two-dimensional 'summary plots'. For those models of SUSY breaking where the squark masses are related to the slepton and ino particle masses, we also examine the constraints in the plane of muon $g-2$ and $\text{Br}(b \to s\gamma)$. The MSSM model points do not appear in those plots since squark masses can be set large to make them consistent with the $\text{Br}(b \to s\gamma)$ constraint.

In the analysis we have performed in Fig. 6, the direction of the minor axis of the ellipse, which corresponds to the most tightly constrained direction, is $-0.799\Delta S_Z + 0.602\Delta T_Z$,

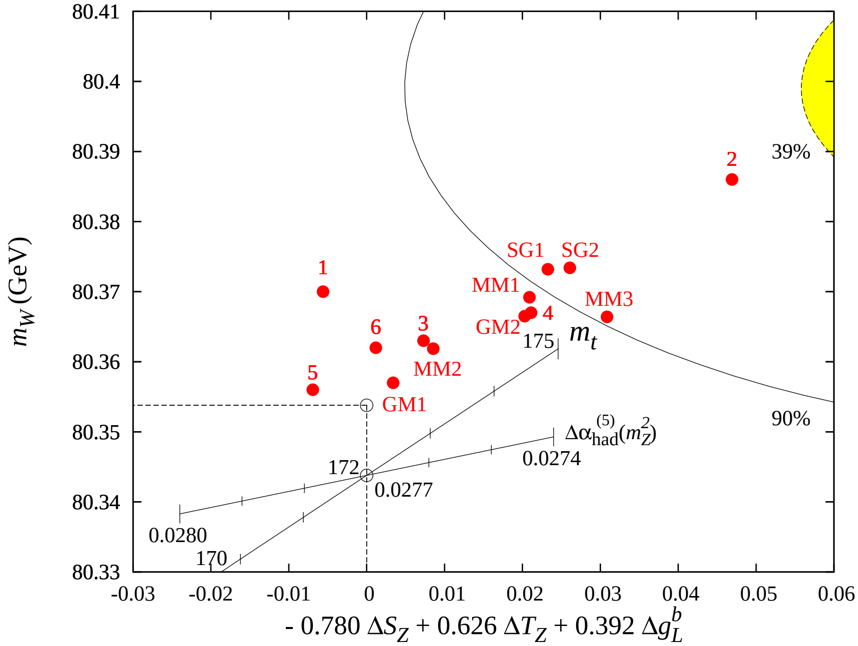

Figure 11: The same as Fig. 10 except that the jet asymmetry data are not included in the analysis.

along which

$$-0.799\Delta S_Z + 0.602\Delta T_Z = 0.016 + 2.07\Delta g_L^b + 0.025x_\alpha \pm 0.036. \tag{37}$$

We can conveniently combine this result with the constraint from m_W in a single figure (Fig. 10). In the figure, the 39% and the 90% CL favored regions are shown as the ellipses. Also shown as the upper open circle is the SM prediction for our reference point, $(m_t, m_{H_{\rm SM}}, \Delta\alpha_{\rm had}^{(5)}(m_Z^2)) = (172\text{GeV}, 120\text{GeV}, 0.0277)$. The SM predictions for different m_t within $169\text{GeV} \leq m_t \leq 175\text{GeV}$ can be read off using the "ruler" around the lower open circle. For example, if we take $m_t = 175\text{GeV}$ instead of $m_t = 172\text{GeV}$, the SM prediction moves from the upper open circle toward the upper-right, in the direction of the vector whose initial point is the lower open circle with the terminal point being the point shown as "175" and also by the length of the same vector. We see that, within the range of the top quark mass shown, a larger top quark mass is favored from the data. This preference for a larger top quark mass is clearer in m_W than in the most constrained combination of ΔS_Z-ΔT_Z.

In Fig. 10, we also plot the sample SUSY points. In the direction of the most constrained ΔS_Z-ΔT_Z combination the fit does not improve very much by introducing SUSY particles since the SM already gives a good description. It is also seen that all our SUSY sample points lie within the 1-σ favored range of this most constrained direction. These tendencies could already be read off in Fig. 6. In the m_W direction, we have improvements in general as discussed in Section 4.3.

We can repeat the same analysis as Fig. 10 also in the case where the jet asymmetry data are not included in the input data. The most constrained direction in the ΔS_Z-ΔT_Z

plane in this case is

$$-0.780\Delta S_Z + 0.626\Delta T_Z = 0.100 - 0.39\Delta g_L^b + 0.024x_\alpha \pm 0.044. \tag{38}$$

Combining this with the constraint from m_W, we show the favored region in Fig. 11. Compared to Fig. 10, we see that the ellipses move toward the right, which is the negative ΔS_Z direction. We also show the SM prediction for the reference point as the upper open circle, which will move according to the "ruler" around the lower open circle for a different m_t. In this case, there is a clearer tendency that the large top quark mass is favored within the range of m_t shown. We also show the predictions from our sample SUSY points. As a general tendency, our SUSY scenarios slightly improve the fit over the SM reference point. In this case, the light slepton scenario, MSSM2, can improve the fit most efficiently among our sample SUSY points, since we have chosen the slepton mass small in such a way that it can better explain the negative ΔS_Z. The degree of the improvement can also be seen in the χ^2 without jet asymmetry data of Tables 6 and 7. At MSSM2, $\chi^2_{\rm min} = 8.30$, which is much better than that of the SM reference point, $\chi^2_{\rm min} = 14.83$, and also than other sample SUSY points.

Having discussed the EW constraints, we now take the constraint from $b \to s\gamma$ into account. The experimental value quoted in RPP 2010 [13] is $\mathrm{Br}(B \to X_s\gamma) = (3.55 \pm 0.26) \times 10^{-4}$, while the SM prediction at NNLO is $\mathrm{Br}(b \to s\gamma) = (3.15 \pm 0.23) \times 10^{-4}$ in Ref. [93], and $\mathrm{Br}(b \to s\gamma) = (2.98 \pm 0.26) \times 10^{-4}$ in Ref. [94]. Since the experimental and the theoretical values agree within 2-σ level, it is preferred that the SUSY contribution is not very large so that it does not spoil the rough agreement.

To suppress the SUSY contributions, we can think of two possibilities: either the relevant SUSY particles are heavy enough, or a cancellation among the relevant diagrams happens. To see how this can be realized, let us look into the structure of the SUSY contributions. At one-loop, the SUSY contribution mainly comes from the chargino–stop loop and the charged-Higgs–top loop diagrams. We neglect the possible contributions from the gluino–sbottom loop diagram, assuming the minimal flavor violation [95]. Under this assumption, we are only interested in those parameter sets in which the chargino–stop and the charged-Higgs–top contributions cancel with each other to the extent that the experimental constraint is satisfied, or those parameter sets in which the relevant SUSY particles are heavy enough.

In Fig. 12 we show the predictions for the muon $g-2$ and $\mathrm{Br}(b \to s\gamma)$ for these sample points. Also shown as the inner and the outer ellipses are the 39% and the 90% CL contours, respectively. In the figure, to specify the favored region of $\mathrm{Br}(b \to s\gamma)$, we use the experimental result $\mathrm{Br}(B \to X_s\gamma) = (3.55 \pm 0.26) \times 10^{-4}$. As for the uncertainty in the Standard Model prediction, we assign 0.26×10^{-4}, which is the larger of the uncertainties in the two SM predictions mentions above. We add the uncertainties in the experimental results and the SM prediction in quadrature. Concerning the MSSM prediction for $\mathrm{Br}(b \to s\gamma)$, we use `micromegas` version 2.0.7 [96], while the SUSY contribution to the muon $g-2$ is calculated by using our own code.

From the figure, concerning $\mathrm{Br}(b \to s\gamma)$, we see that all the points are within the 90% CL favored region. We also see that $\mathrm{Br}(b \to s\gamma)$ at SG1 is a little bit farther from the central point than the other points. This happens since, at SG1, the third generation squarks and the lighter charginos are slightly lighter than those of the other points, and since the cancellation among the SUSY diagrams are milder.

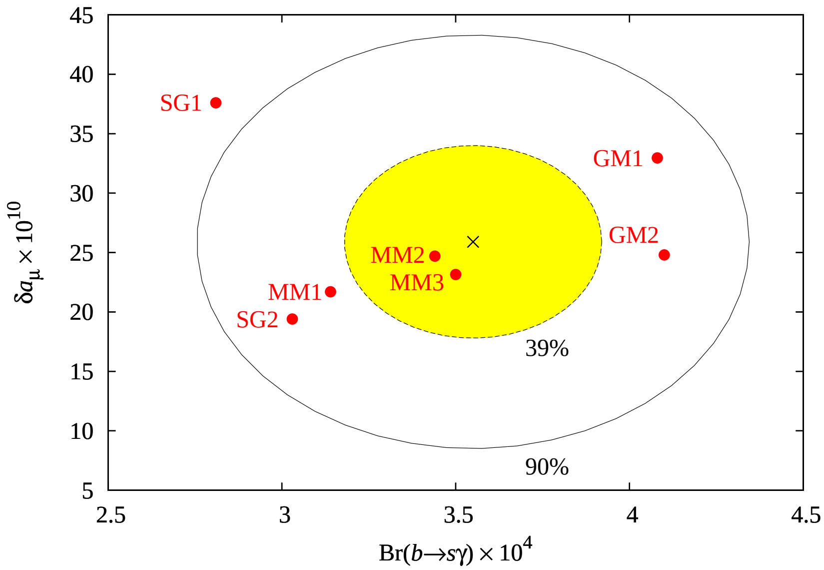

Figure 12: The branching ratio of $b \to s\gamma$ and the SUSY contribution to the muon $g-2$ at our sample points. The inner and the outer ellipses stand for the 39% and the 90% CL favored regions, respectively.

Concerning the muon $g-2$ for those sample points, since we have already discussed in Section 2, we do not repeat it here.

As an additional constraint on these SUSY sample points, we now comment on the dark matter relic density predicted from these models. At all our SUSY sample parameters, the lightest SUSY particle (LSP) is stable because of the R-parity conservation, and hence the LSP is a potential candidate for dark matter. The LSP is the lightest neutralino in our sample points based on mSUGRA or the mirage mediation (MM), while those based on the gauge-mediated models the LSP is gravitino. In either cases, the relic density of the LSP is calculable. For the mSUGRA and MM based points, we have calculated the LSP relic density using `micromegas`. The results are $\Omega h^2 = 0.08$, 0.01, 0.11, 0.08 and 0.001 for SG1, SG2, MM1, MM2 and MM3, respectively. For all these cases except MM3, the LSP is an almost pure bino, with a very small mixture from Higgsinos and wino. For MM3, since the LSP is wino, the relic density is smaller because of the larger annihilation cross section of the wino LSP. As for the gauge mediated model sample points, GM1 and GM2, the LSP mass, namely the gravitino mass, is in the eV range, in which case the LSP relic density is negligible. These relic densities should be compared to the results of a global fit of the cosmological parameters on the non-baryonic matter density $\Omega_{\rm DM} h^2$ [13],

$$\Omega_{\rm DM} h^2 = 0.110 \pm 0.006. \tag{39}$$

We see that for all our sample points, the relic density of the LSP is nearly equal to or less than the observed density of dark matter. If the relic density of the LSP were significantly larger than the value in Eq. (39), those models would be excluded. On the contrary, if the relic density of the LSP is less than the value in Eq. (39), such a model can still be phenomenologically viable since there is still a possibility that an unknown particle like an

axion can also contribute to the dark matter density. Hence we conclude that our sample parameters are not excluded from the dark matter density calculations.

We do not include constraints from the low-Q^2 precision measurements such as atomic parity violation and neutrino-nucleon scatterings at low energies since constraints from these measurements are known to be much less stringent than those from the Z-pole experiments. Another class of observables we do not include is those from B-physics, namely $\mathrm{Br}(B_s^0 \to \mu^+\mu^-)$, $\mathrm{Br}(B^+ \to \tau^+\nu_\tau)$ and Δm_s. Even though these observables potentially give non-trivial constraints on large $\tan\beta$ models [97], we do not include them since our main interest in the present paper is in the signal from the slepton and the ino sectors rather than the squark and the Higgs sectors.

6 Summary

We have studied impacts of recent muon $g-2$ measurements and the LEP final electroweak data on the MSSM. We identify several regions of the MSSM parameter space which fill the gap between the SM prediction and the observed value of the muon $g-2$, and at the same time have observable effects for the electroweak precision measurements. In all the selected regions of the MSSM parameter space, the MSSM predictions are consistent with the LEP/SLC Z boson observables, while improve the SM fit to the W boson mass slightly. When we remove the constraints from the jet asymmetry measurements at LEP/SLC, we find that MSSM models with very light sleptons ($\lesssim$ 200 GeV) and moderately heavy ino particles ($\sim$ several 100 GeV) are favored over models with a very light chargino ($\sim$ 100 GeV) and moderately light sleptons ($\sim$ a few 100 GeV).

We also examined a few models of SUSY breaking scenarios, including minimal SUGRA models, gauge mediation models, and the mixed moduli and anomaly mediation models. All of them have parameter region with relatively light slepton and ino particles which contribute to the muon $g-2$. Those models with moderately heavy smuons and ino particles can still contribute to the muon $g-2$ with large $\tan\beta$ ($\gtrsim$ 40), and can at the same time improve the fit to m_W and the Z boson parameters if there is a significant mixing in the stau sector. Sample scenarios in each SUSY breaking models are found which improves the SM fit to the muon $g-2$, m_W, the Z parameters in the absence of jet asymmetry data, and are still compatible with $\mathrm{Br}(b \to s\gamma)$. We believe that our investigations will help us identifying the supersymmetry breaking scenario once signatures of SUSY particle productions are discovered at the LHC.

Acknowledgements

We thank Y. Shimizu for providing us with the SUSY parameters for the sample point GM1, and A. Crivellin, J. Girrbach and U. Nierste for comments on the large A-term scenario and on the effect of $\tan\beta$-enhanced resummation. KH wishes to thank Aspen Center for Physics where stimulating discussions with the participants of the 2008 summer program took place. DN would like to thank K. Okumura for useful discussions on the mirage mediation models. This work is supported in part by Grants-in-Aid for Scientific Research (No. 18340060 and 20340064) from the Japan Society for the Promotion of Science (JSPS).

References

[1] G.C. Cho and K. Hagiwara, Nucl. Phys. **B574**, 623 (2000).

[2] The LEP Collaborations ALEPH, DELPHI, L3, OPAL, the LEP Electroweak Working Group and the SLD Heavy Flavour and Electroweak Groups, CERN-EP/99-15.

[3] The ALEPH, DELPHI, L3, OPAL, SLD Collaborations, the LEP Electroweak Working Group, the SLD Electroweak and Heavy Flavour Groups, Phys. Rept. **427**, 257 (2006).

[4] LEP Electroweak Working Group, `http://lepewwg.web.cern.ch/LEPEWWG/`.

[5] J. Z. Bai *et al.* [BES Collaboration], Phys. Rev. Lett. **84**, 594 (2000); Phys. Rev. Lett. **88**, 101802 (2002).

[6] M. Ablikim *et al.* [BES Collaboration], Phys. Lett. **B677**, 239 (2009).

[7] G. W. Bennett *et al.* [Muon $g-2$ Collaboration], Phys. Rev. **D73**, 072003 (2006).

[8] T. Teubner, talk at the 11th International Workshop on Tau Lepton Physics (Tau 2010), Manchester, September 13-17, 2010.

[9] M. Davier, A. Hoecker, B. Malaescu and Z. Zhang, Eur. Phys. J. **C71**, 1515 (2011).

[10] F. Jegerlehner and R. Szafron, Eur. Phys. J. **C71**, 1632 (2011).

[11] F. Jegerlehner and A. Nyffeler, Phys. Rept. **477**, 1 (2009).

[12] V. M. Abazov *et al.* [D0 collaboration], Phys. Rev. Lett. **103**, 141801 (2009); Phys. Rev. **D66**, 012001 (2002); J. Abdallah *et al.* [DELPHI collaboration], Eur. Phys. J. **C55**, 1 (2008); T. Aaltonen *et al.* [CDF collaboration], Phys. Rev. Lett. **99**, 151801 (2007); Phys. Rev. **D77**, 112001 (2007); G. Abbiendi *et al.* [OPAL collaboration], Eur. Phys. J. **C45**, 307 (2006); P. Achard *et al.* [L3 collaboration], Eur. Phys. J. **C45**, 569 (2006); S. Schael *et al.* [ALEPH collaboration], Eur. Phys. J. **C47**, 309 (2006).

[13] K. Nakamura *et al.* [Particle Data Group], J. Phys. **G 37**, 075021 (2010).

[14] T. Aaltonen *et al.* [CDF collaboration], Phys. Rev. **D79**, 072001 (2009); Phys. Rev. **D79**, 072010 (2009); Phys. Rev. Lett. **102**, 152001 (2009); V. M. Abazov *et al.* [D0 collaboration], Phys. Rev. **D80**, 092006 (2009); Phys. Rev. Lett. **101**, 182001 (2008); Nature **429**, 638 (2004); A. Abulencia *et al.* [CDF collaboration], Phys. Rev. **D75**, 071102R (2007); T. Affolder *et al.* [CDF collaboration], Phys. Rev. **D63**, 032003 (2001); F. Abe *et al.* [CDF collaboration], Phys. Rev. Lett. **82**, 271 (1999); Phys. Rev. Lett. **82**, 2808 (1999) (E); Phys. Rev. Lett. **79**, 1992 (1997); B. Abbott *et al.* [D0 collaboration], Phys. Rev. Lett. **80**, 2063 (1998).

[15] S. Heinemeyer, W. Hollik and G. Weiglein, Phys. Rept. **425**, 265 (2006); M. J. Ramsey-Musolf and S. Su, Phys. Rept. **456**, 1 (2008).

[16] J. Erler, Phys. Rev. **D81**, 051301 (2010).

[17] J. Ellis, J. R. Espinosa, G. F. Giudice, A. Hoecker and A. Riotto, Phys. Lett. **B679**, 369 (2009).

[18] H. Flacher, M. Goebel, J. Haller, A. Hocker, K. Moenig and J. Stelzer, Eur. Phys. J. **C60**, 543 (2009).

[19] S. Heinemeyer, W. Hollik, A. M. Weber and G. Weiglein, JHEP **0804**, 039 (2008).

[20] A. Djouadi, P. Gambino, S. Heinemeyer, W. Hollik, C. Junger and G. Weiglein, Phys. Rev. Lett. **78**, 3626 (1997); Phys. Rev. **D57**, 4179 (1998); S. Heinemeyer and G. Weiglein, JHEP **0210**, 072 (2002); J. Haestier, S. Heinemeyer, D. Stockinger and G. Weiglein, JHEP **0512**, 027 (2005); S. Heinemeyer, W. Hollik, D. Stockinger, A. M. Weber and G. Weiglein, JHEP **0608**, 052 (2006).

[21] B. C. Allanach, T. J. Khoo, C. G. Lester, S. L. Williams, JHEP **1106**, 035 (2011).

[22] B. C. Allanach, Phys. Rev. **D83**, 095019 (2011).

[23] O. Buchmueller, R. Cavanaugh, D. Colling, A. De Roeck, M. J. Dolan, J. R. Ellis, H. Flacher, S. Heinemeyer *et al.*, Eur. Phys. J. **C71**, 1583 (2011).

[24] M. E. Cabrera, A. Casas and R. R. de Austri, JHEP **1005**, 043 (2010).

[25] Y. Akrami, P. Scott, J. Edsjo, J. Conrad and L. Bergstrom, JHEP **1004**, 057 (2010).

[26] O. Buchmueller *et al.*, Eur. Phys. J. **C64**, 391 (2009).

[27] P. Bechtle, K. Desch, M. Uhlenbrock and P. Wienemann, Eur. Phys. J. **C66**, 215 (2010).

[28] S. S. AbdusSalam, B. C. Allanach, M. J. Dolan, F. Feroz and M. P. Hobson, Phys. Rev. **D80**, 035017 (2009).

[29] F. Feroz, M. P. Hobson, L. Roszkowski, R. Ruiz de Austri and R. Trotta, arXiv:0903.2487 [hep-ph].

[30] R. Trotta, F. Feroz, M. P. Hobson, L. Roszkowski and R. Ruiz de Austri, JHEP **0812**, 024 (2008).

[31] O. Buchmueller *et al.*, JHEP **0809**, 117 (2008).

[32] F. Feroz, B. C. Allanach, M. Hobson, S. S. AbdusSalam, R. Trotta and A. M. Weber, JHEP **0810**, 064 (2008).

[33] S. Heinemeyer, X. Miao, S. Su and G. Weiglein, JHEP **0808**, 087 (2008).

[34] O. Buchmueller *et al.*, Phys. Lett. **B657**, 87 (2007).

[35] J. R. Ellis, S. Heinemeyer, K. A. Olive, A. M. Weber and G. Weiglein, JHEP **0708**, 083 (2007).

[36] L. Roszkowski, R. R. de Austri and R. Trotta, JHEP **0704**, 084 (2007).

[37] B. C. Allanach, C. G. Lester and A. M. Weber, JHEP **0612**, 065 (2006).

[38] J. R. Ellis, S. Heinemeyer, K. A. Olive and G. Weiglein, JHEP **0605**, 005 (2006).

[39] R. R. de Austri, R. Trotta and L. Roszkowski, JHEP **0605**, 002 (2006).

[40] B. C. Allanach, Phys. Lett. **B635**, 123 (2006).

[41] B. C. Allanach and C. G. Lester, Phys. Rev. **D73**, 015013 (2006).

[42] G. Marandella, C. Schappacher and A. Strumia, Nucl. Phys. **B715**, 173 (2005).

[43] J. R. Ellis, S. Heinemeyer, K. A. Olive and G. Weiglein, JHEP **0502**, 013 (2005).

[44] J. R. Ellis, K. A. Olive, Y. Santoso and V. C. Spanos, Phys. Rev. **D69**, 095004 (2004).

[45] W. de Boer and C. Sander, Phys. Lett. **B585**, 276 (2004).

[46] A. Djouadi, M. Drees and J. L. Kneur, JHEP **0108**, 055 (2001).

[47] J. Erler and D. M. Pierce, Nucl. Phys. **B526**, 53 (1998).

[48] S. P. Martin, K. Tobe and J. D. Wells, Phys. Rev. **D71**, 073014 (2005).

[49] B. Fuks, B. Herrmann and M. Klasen, Nucl. Phys. **B810**, 266 (2009).

[50] B. C. Allanach, M. J. Dolan and A. M. Weber, JHEP **0808**, 105 (2008).

[51] G. Belanger, F. Boudjema, A. Cottrant, A. Pukhov and A. Semenov, Nucl. Phys. **B706**, 411 (2005).

[52] L. Roszkowski, R. Ruiz de Austri, R. Trotta, Y. L. Tsai and T. A. Varley, arXiv:0903.1279 [hep-ph].

[53] S. S. AbdusSalam, B. C. Allanach, F. Quevedo, F. Feroz and M. Hobson, Phys. Rev. **D81**, 095012 (2010).

[54] A. Kurylov, M. J. Ramsey-Musolf and S. Su, Phys. Rev. **D68**, 035008 (2003).

[55] A. Kurylov, M. J. Ramsey-Musolf and S. Su, Nucl. Phys. **B667**, 321 (2003).

[56] G. Altarelli, F. Caravaglios, G. F. Giudice, P. Gambino and G. Ridolfi, JHEP **0106**, 018 (2001).

[57] K. Hagiwara and G. Kirilin, JHEP **1010**, 093 (2010).

[58] P. J. Mohr, B. N. Taylor and D. B. Newell, Rev. Mod. Phys. **80**, 633 (2008).

[59] B. Aubert *et al.* [BaBar Collaboration], Phys. Rev. Lett. **103**, 231801 (2009).

[60] R. R. Akhmetshin *et al.* [CMD-2 Collaboration], JETP Lett. **84** (2006) 413; Phys. Lett. **B648**, 28 (2007); V. M. Aulchenko *et al.* [CMD-2 Collaboration], JETP Lett. **82** (2005) 743.

[61] F. Ambrosino *et al.* [KLOE Collaboration], Phys. Lett. **B670**, 285 (2009).

[62] F. Ambrosino *et al.* [KLOE Collaboration], Phys. Lett. **B700**, 102 (2011).

[63] M. N. Achasov *et al.* [SND Collaboration], J. Exp. Theor. Phys. **101**, 1053 (2005); J. Exp. Theor. Phys. **103**, 380 (2006).

[64] J. Prades, E. de Rafael and A. Vainshtein, arXiv:0901.0306 [hep-ph].

[65] P. von Weitershausen, M. Schafer, H. Stockinger-Kim and D. Stockinger, Phys. Rev. **D81**, 093004 (2010); S. Marchetti, S. Mertens, U. Nierste and D. Stockinger, Phys. Rev. **D79**, 013010 (2009); S. Heinemeyer, D. Stockinger and G. Weiglein, Nucl. Phys. **B699**, 103 (2004); Nucl. Phys. **B690**, 62 (2004).

[66] J. Girrbach, S. Mertens, U. Nierste and S. Wiesenfeldt, JHEP **1005**, 026 (2010); A. Crivellin, L. Hofer and J. Rosiek, JHEP **1107**, 017 (2011).

[67] G. C. Cho, K. Hagiwara and M. Hayakawa, Phys. Lett. **B478**, 231 (2000).

[68] G. C. Cho and K. Hagiwara, Phys. Lett. **B514**, 123 (2001).

[69] K. Choi, K. S. Jeong and K. i. Okumura, JHEP **0509**, 039 (2005); M. Endo, M. Yamaguchi and K. Yoshioka, Phys. Rev. **D72**, 015004 (2005). A. Falkowski, O. Lebedev and Y. Mambrini, JHEP **0511**, 034 (2005).

[70] A. Crivellin, J. Girrbach and U. Nierste, Phys. Rev. **D83**, 055009 (2011).

[71] LEP SUSY Working Group, `http://lepsusy.web.cern.ch/lepsusy/`

[72] M. Drees and K. Hagiwara, Phys. Rev. **D42**, 1709 (1990).

[73] L. J. Hall, J. D. Lykken and S. Weinberg, Phys. Rev. **D27**, 2359 (1983).

[74] M. Dine and A. E. Nelson, Phys. Rev. **D48**, 1277 (1993); M. Dine, A. E. Nelson and Y. Shirman, Phys. Rev. **D51**, 1362 (1995); M. Dine, A. E. Nelson, Y. Nir and Y. Shirman, Phys. Rev. **D53**, 2658 (1996).

[75] K. Choi, A. Falkowski, H. P. Nilles and M. Olechowski, Nucl. Phys. **B718**, 113 (2005). K. Choi, A. Falkowski, H. P. Nilles, M. Olechowski and S. Pokorski, JHEP **0411**, 076 (2004).

[76] J. A. Aguilar-Saavedra *et al.*, Eur. Phys. J. **C46**, 43 (2006).

[77] B. C. Allanach *et al.*, *"The Snowmass points and slopes: Benchmarks for SUSY searches,"* in *Proc. of the APS/DPF/DPB Summer Study on the Future of Particle Physics (Snowmass 2001)* ed. N. Graf, *In the Proceedings of APS / DPF / DPB Summer Study on the Future of Particle Physics (Snowmass 2001), Snowmass, Colorado, 30 Jun - 21 Jul 2001, pp P125* [arXiv:hep-ph/0202233].

[78] J. Hisano and Y. Shimizu, Phys. Lett. **B655**, 269 (2007).

[79] S. Kachru, R. Kallosh, A. Linde and S. P. Trivedi, Phys. Rev. **D68**, 046005 (2003).

[80] K. Choi, K. S. Jeong, T. Kobayashi and K. i. Okumura, Phys. Rev. **D75**, 095012 (2007).

[81] H. Abe, T. Higaki and T. Kobayashi, Phys. Rev. **D73**, 046005 (2006).

[82] M. Casolino *et al.* [PAMELA Collaboration], arXiv:0810.4980 [astro-ph].

[83] O. Adriani *et al.* [PAMELA Collaboration], Nature **458**, 607 (2009).

[84] P. Grajek, G. Kane, D. Phalen, A. Pierce and S. Watson, Phys. Rev. **D79**, 043506 (2009).

[85] K. Hagiwara, Ann. Rev. Nucl. Part. Sci. **48**, 463 (1998).

[86] The LEP Collaborations (ALEPH, DELPHI, L3, OPAL), the LEP Electroweak Working Group and the SLD Heavy Flavor Group, CERN-EP/2001-021 [arXiv:hep-ex/0103048].

[87] K. Hagiwara, D. Haidt, C.S. Kim and S. Matsumoto, Z. Phys. **C64**, 559 (1994) [Erratum-ibid. **C68**, 352 (1995)].

[88] M. E. Peskin and T. Takeuchi, Phys. Rev. Lett. **65**, 964 (1990); Phys. Rev. **D46**, 381 (1992).

[89] K. Hagiwara, D. Haidt and S. Matsumoto, Eur. Phys. J. **C2**, 95 (1998).

[90] A. Czarnecki and J. H. Kuhn, Phys. Rev. Lett. **77**, 3955 (1996); R. Harlander, T. Seidensticker and M. Steinhauser, Phys. Lett. **B426**, 125 (1998); J. Fleischer, F. Jegerlehner, M. Tentyukov and O. Veretin, Phys. Lett. **B459**, 625 (1999).

[91] A. B. Arbuzov *et al.*, Comput. Phys. Commun. **174**, 728 (2006); D. Y. Bardin *et al*, Comput. Phys. Commun. **133**, 229 (2001).

[92] C. W. Bauer, S. Fleming, D. Pirjol and I. W. Stewart, Phys. Rev. **D63**, 114020 (2001); M. Beneke, A. P. Chapovsky, M. Diehl and T. Feldmann, Nucl. Phys. **B643**, 431 (2002).

[93] M. Misiak *et al.*, Phys. Rev. Lett. **98**, 022002 (2007).

[94] T. Becher and M. Neubert, Phys. Rev. Lett. **98**, 022003 (2007).

[95] E. Gabrielli and G. F. Giudice, Nucl. Phys. **B433**, 3 (1995) [Erratum-ibid. **B507**, 549 (1997)].

[96] G. Belanger, F. Boudjema, A. Pukhov and A. Semenov, Comput. Phys. Commun. **176**, 367 (2007); Comput. Phys. Commun. **174**, 577 (2006); Comput. Phys. Commun. **149**, 103 (2002).

[97] M. Bona *et al.* [UTfit Collaboration], Phys. Lett. **B687**, 61 (2010).